# Dissolved greenhouse gases (nitrous oxide and methane) associated with the naturally iron-fertilized Kerguelen region (KEOPS 2 cruise) in the Southern Ocean

**L. Farías[1]*, L. Florez-Leiva[2], V. Besoain[1,3], G. Sarthou[4], and C. Fernández[5]**

[1] Departamento de Oceanografía. Universidad of Concepción and Centro de Ciencia del Clima y la Resiliencia (CR)[2], Chile

[2] Programa de Biología. Universidad del Magdalena, Santa Marta, Colombia

[3] Escuela de Ciencias del Mar, Pontificia Universidad Católica de Valparaíso, Chile

[4]LEMAR-UMR 6539, CNRS-UBO-IRD-IFREMER, Place Nicolas Copernic, 29280 Plouzané, France

[5]Sorbonne Universités, UPMC Univ Paris 06, UMR 7621, Laboratoire d'Océanographie Microbienne, Observatoire Océanologique, F-66650 Banyuls/mer, France and Department of Oceanography, COPAS SA program and Interdisciplinary Center for Aquaculture Research (INCAR), University of Concepción, Chile

Correspondence should be addressed to:

Laura Farias; lfarias @profc.udec.cl

## ABSTRACT

The concentrations of greenhouse gases (GHGs) like nitrous oxide ($N_2O$) and methane ($CH_4$) were measured in the Kerguelen Plateau Region (KPR), an area with an annual microalgal bloom caused by natural Fe fertilization, which may stimulate microbes involved in GHG cycling. This study was carried out during the KEOPS 2 cruise during the austral spring of 2011. Oceanographic variables including $N_2O$ and $CH_4$ (from surface to 500 m depth) were sampled in two transects along and across the KRP, the north-south (N-S) transect (46°-51°S, ~72°E) and the west-east (W-E) transect (66°-75°E, ~48.3°S ); both associated with the presence of a plateau, polar fronts and other mesoscale features. The W-E transect had $N_2O$ levels ranging from equilibrium (105%) to slight supersaturation (120%) with respect to the atmosphere. $CH_4$ levels fluctuated dramatically, with high supersaturations (120-970%) in areas close to the coastal waters of Kerguelen Island and in the polar front (PF). The N-S transect showed a more homogenous distribution for both gases, with $N_2O$ and $CH_4$ levels from 88% to 171% and 45% to 666% saturation, respectively, but surface $CH_4$ peaked at southeastern stations of the KPR (A3 stations), where a phytoplankton bloom was observed. Both gases responded significantly, but in contrasting ways ($CH_4$ accumulation and $N_2O$ depletion), to the patchy distribution of particulate matter as chlorophyll a. This seems to be strongly stimulated by Fe supply from different sources. Air-sea fluxes for $N_2O$ (from -10.5 to 8.65, mean 1.71 µmol $m^{-2}$ $d^{-1}$) and for $CH_4$ (from 0.32 to 38.1, mean 10.07 µmol $m^{-2}$ $d^{-1}$) indicated that the KPR is both a sink and a source for $N_2O$, and a considerable and variable source for $CH_4$. These results are previously unreported for the Southern Ocean and it is suggested that it may be caused by an intense microbial $CH_4$ production.


**Keywords**: Nitrous oxide, methane, dissolved iron fertilized Kerguelen area, mesoscale structures and polar front Southern Ocean.

## 1. Introduction

The increasing concentration of greenhouse gases (GHGs) in the troposphere, such as $CO_2$, $N_2O$ and $CH_4$, affect the Earth's radiative balance. Additionally, the increasing concentration of ozone-depleting gases (such as chlorofluorocarbons and $N_2O$) in the stratosphere is weakening the ozone shield, permitting higher levels of damaging ultraviolet radiation to reach the Earth's surface. The strength of each GHG is determined by its respective residence time in the atmosphere (Cicerone and Orelamland, 1988) and the magnitude of emissions to the atmosphere, of which the oceans make an important contribution (IPCC, 2007).

Although oceans are generally considered to be a net source of GHGs to the atmosphere, such as $N_2O$ and $CH_4$, the oceanic distribution of these GHGs and the amount of exchanged via the air-sea interface is highly variable (Nevison et al., 1995; Holmes et al., 2000; Rhee et al., 2009). Thus, source and sink behaviors of GHGs have been observed on different spatial and temporal scales. In general terms, these behaviors depend on biological and physical processes that promote outgassing or sequestering mechanisms. Physical and biological features of the Southern Ocean suggest the existence of a potential for both the production and removal of $CH_4$ and $N_2O$ (Rees et al., 1999; Tilbrook and Karl, 1994), although very little information on dissolved $N_2O$ and $CH_4$ distributions is currently available for the region. The substantial spatial variation in regional gas exchange could be due to the increased gas solubility in low-temperature Sub- and Antarctic waters, combined with either the downwelling associated with intermediate and deep water formation over the convergence band (Antarctic Polar Frontal Zone or "PFZ"), or the low-temperature Antarctic waters, along with the upwelling of deep and intermediate waters in the southern part of the PFZ (Parker and Viver, 2012).

In different regions of the Southern Ocean, the surface layer is always supersaturated with $CH_4$ (Bates et al. 1996; Tilbrook and Karl, 1994, Toshida et al., 2011), but this is not the case for $N_2O$ that is observed

in an under- or super saturated condition ( Law and Ling, 2001, Rees et al., 1997, Zhan and Chen, 2009). Aside from physical processes affecting GHG concentrations in the water column and their concomitant air-sea fluxes, they additionally depend on organic matter (OM) availability and oxygen levels, which determine whether aerobic or anaerobic OM respiration occurs (Codispoti et al., 2001; Reeburgh, 2007). The availability of dissolved iron (dFe) should also be included as a variable affecting GHG cycling; directly as several Fe-containing enzymes, which are involved in the electron transfer chains in bacterial respiratory systems and Nitrogen cycling, are required for GHG cycling (Arrieta et al, 2004; Kirchman et al., 2003; Morel et al., 2003a) and, indirectly as dFe stimulates ocean productivity which can enhance carbon and nitrogen export from the euphotic zone to the subsurface (Boyd and Ellwood, 2010), resulting in a an increase of the microbial activities which may mediate GHG via nitrification (Fuhrman and Capone , 1991),

$N_2O$ is mainly produced during the first step of nitrification; the aerobic oxidation of $NH_4^+$ to $NO_2^-$, and during partial denitrification, the anaerobic reduction of $NO_3^-/NO_2^-$ to $N_2O$. $N_2O$ can also be consumed by complete denitrification via dessimilatory reduction to $N_2$ (Codispoti and Cristiensen, 1985) or assimilatory $N_2O$ reduction to $NH_4^+$ (Farias et al 2013). $CH_4$, on the other hand, is mainly formed by methanogens during anaerobic OM degradation (Wuebble & Hayboe, 2001) or by methylotrophs during $CH_4$ formation derived from transformations of methyl-compounds such as methylphosphonate (MPn) (Karl et al., 2008), dimethyl-sulphoniopropionate (DMSP) (Damm et al., 2010) and dimethylsulphide (DMS) (Florez-Leiva et al., 2013). In addition, $CH_4$ can be consumed (oxidized) via aerobic methanothophy (Hanson and Hanson, 1996). Since Southern Ocean waters are well oxygenated, $N_2O$ formed by nitrification (Nevison et al., 2003) and $CH_4$ formed by either methanogenesis in suspended particles (Scranton and Brewer 1977) or by methylotrophy, are thought to be the dominant mechanisms of production in surface waters (Sun et al., 2011).

The main objective of the present study is to describe for first time the $N_2O$ and $CH_4$ contents in the Southern Ocean under the influence of natural fertilization events during the spring phytoplankton bloom in the KPR. The determination of the role of the Southern Ocean in $CH_4$ and $N_2O$ air–sea exchange may be critical in understanding the factors/variables that influence GHG cycling. This includes dFe which comes from different sources within the KPR, inducing mesotrophic conditions that are associated with the coastal waters of Kerguelen Island, the area of quasi permanent phytoplanktonic bloom in the Central Plateau area of the KPR( Blain et al., 2008; Chever et al., 2010), and with the Antarctic Polar front and other mesoscale structures (Mongin et al., 2008, Lasbleiz et al., 2014).

## 2. Methods

### 2.1. Study area

Samples were collected within the Kerguelen Plateau Region or KPR (Fig. 1) during the KEOPS 2 cruise at stations along north to south (TNS,46°–51°S) and west to east (TWE, 66–75°E)transects. The cruise was carried out from October 11$^{th}$ to December 11$^{th}$, 2011, on board the research vessel (RV) *Marion-Dufresne*. Some of the sample stations were located in the PFZ in the coastal shelf waters of Kerguelen Island and within the southeastern KPR bloom (including station A3 from the previous KEOPS 1 cruise), which are naturally Fe-enriched, however another station was sampled (St. R), which is located beyond the KPR and considered to be representative of the HNLC area off the KPR (see Table 1). The hydrographic condition of the sampling stations was selected according to a strategy based on real-time ocean color and altimetry satellite images (d´Ovidio et al., 2012).

**2.2. Continuous and discrete sampling:** Continuous vertical profiles of temperature, salinity, dissolved $O_2$, fluorescence and photosynthetically active radiation (PAR) were obtained using a conductivity temperature and depth (CTD) sensor. Water was sampled with a CTD-Rosette sampler (SBE 32 24x10-L Carousel Water Sampler with 10-L Niskin bottles). Water samples for gases ($N_2O$, $CH_4$), nutrients,

and pigments (sampled in this correlative order) were obtained from nine depths distributed between the surface and a 500m depth. Water samples for $CH_4$ (triplicate) and $N_2O$ (triplicate) analyses were taken in 20 mL glass vials and poisoned with $HgCl_2$ (0.1 ml of saturated $HgCl_2$ solution per vial). The vials were then sealed with a butyl-rubber septum and aluminum cap, avoiding bubble formation, and stored at room temperature in darkness until laboratory analysis. Syringes of 50 mL were directly connected to the spigot of the Niskin bottles to take nutrient samples ($NO_3^-$, $NO_2^-$ , $PO_4^{3-}$ and $Si(OH)_4$) at each sampled depth. Duplicate samples were collected and drawn through a 0.45 μm Uptidisc adapted to the syringe, and then immediately analyzed using an autoanalyzer (more details in Blain et al, this volume). Total chlorophyll-a (*TChl-a*) samples in triplicate were filtered into a 25 mm glass- fiber filter (GF/F), and then immediately frozen (-20ºC). Samples were kept until later analysis by high performance liquid chromatography (HPLC) (more details in Lasbleiz et al., 2014).

**2.3. Chemical analysis**: $N_2O$ and $CH_4$ were analyzed by creating into the vial 5 mL of ultra-pure Helium headspace throughout a gastight syringe, followed by an equilibration of gas and liquid phase in the vial at 40°C, and then quantifying gases by a gas chromatograph determined by helium (He) equilibration (5-mL helium headspace and 15-mL of seawater) at 40°C in the vial, followed by quantification via chromatography. $N_2O$ was analyzed in a Varian 3380 Gas Chromatograph using an electron capture detector at 350°C and connected to an autosampler device. $CH_4$ was analyzed in a Schimadzu 17A gas chromatograph using a flame ionization detector at 250°C through a capillary column GS-Q at an oven temperature of 30º C. A calibration curve was made with four concentrations for $N_2O$ (0.1 ppm, 0.32, 0.5 ppm, and 1 ppm, by Matheson standards) and four concentrations for $CH_4$ (0.5, 1.78, 2 and 10 ppm, by Matheson standards). Both detectors linearly responded to these concentration ranges. The analytical error for the $N_2O$ and $CH_4$ analyses was less than 3% and 5% respectively. The samples were taken in triplicate in 20 mL vials and carefully sealed to avoid air

bubbles. They were then preserved with 50 µL of saturated $HgCl_2$ and stored in darkness until analysis. The ECD and FID detectors lineally responded to these concentration ranges and the analytical error for the $N_2O$ measurements for this study was about 3%. The uncertainty of the measurements was calculated from the standard deviation of the triplicate measurements by depth. Samples with a variation coefficient higher than 10 % were not taken into account for the gas database.

More details regarding the analysis of both gases can be found in Farias et al. (2009). Nutrients were immediately analyzed onboard by standard automated colorimetric methods (Tréguer and LeCorre, 1975) using the continuous flow autoanalyser (Skalar). The precision and detection limit of the method was, respectively, ±50 nM and 20 nM for NO3-, and ±30 nM and 110 nM for $PO_4^-$ (more details in Blain et al. this volume). $NH_4^+$ was measured by fluorometric analysis (Holmes et al., 2000) with a precision of ±50 nM.

**2.4. Data analysis**: To interpret the vertical variation of $N_2O$ and $CH_4$ and how biogeochemical processes may affect their concentrations, the water column was divided into two layers according to density gradient: (1) well-mixed and (2) subsurface from the base of the mixed layer (ML) to 500 m (arbitrary depth used only for comparison proposes). Nutrient inventories for T*Chl-a*, $N_2O$ and $CH_4$ were calculated by numerical integration of data at one meter (linear interpolation) increments based on at least 4-6 sampled depths per layer. Saturation percentages of gases were calculated from the measured $CH_4$ and $N_2O$ concentrations and those estimated to be in equilibrium with the current gas concentrations in the atmosphere (NOAA register (http://www.esrl.noaa.gov/gmd/hats/combined /$N_2O$.html), based on *in situ* temperature and salinity according to the solubility parameterization $CH_4$ (Wiesenburg and Guinasso, 1979) and $N_2O$ (Weiss and Price, 1980). GHG flux through the air-sea interface was determined using the following equation, modified by Wanninkhof (1992):

$$F = kw(T°, salinity) \cdot (C_w - C_a)$$

where *kw* is the transfer velocity from the ML to the atmosphere, as a function wind speed, temperature and salinity in the ML according to parametrization, $C_w$ is the mean gas concentration in the mixed layer, while $C_a$ is the gas concentration in the mixed layer expected to be in equilibrium with the atmosphere. Since gas transfer velocity is related to wind speed, this was calculated according to the well-known exchange models of Liss and Merlivat (1986) or LM86 and Wanninkhof (1992) or W92, based on the dependence of the transfer velocity on wind speed. Wind speed and direction were obtained from an onboard register using the ship's meteorological station as per international protocols. Wind speed was estimated as a moving average of seven days before the sampling (stations) in order to smooth out short-term fluctuations and highlight longer-term trends. The mixed layer depth was calculated using a potential density-based criterion, defining the mixed layer depth (ML) as the shallowest depth at which density increased by 0.02 kg $m^{-3}$ from the sea surface value.

Pearson product-moment correlations (rs) were determined for GHG, and T*Chl-a* and nutrient inventories were estimated in the ML and in the whole water column from surface to 500 m depth. The threshold value for statistical significance was set as $p < 0.05$. A principal component analysis (PCA) using the empirical orthogonal function (EOF; Emery and Thomson, 1997) was performed to find the co-variability patterns of a number of stations located in spatial gradients in terms of nutrients, gases ($O_2$, $N_2O$, and $CH_4$), T*Chl-a*, and dFe. This analysis excluded the stations from the NS transect as no measurements were recorded (Quéroué et al, this volume). PCA were made with all biogeochemical variables measured in the ML and with these variables obtained in the water column from the surface to a depth of 500 m, in order to discern differences in the vertical structure.

## Results

### 3.1. Oceanographic conditions.

Oceanographic characteristics of the sampled stations during the KEOPS 2 cruise are shown in Table 1. Two transects, almost synoptically made across and along the KPR (survey region – Fig. 1) were undertaken to establish the position of the main mesoscale structures as fronts (Figure 2). The Polar Front (PF) crosses the KPR and demarcates certain physical structures (convergence process) visible throughout temperature and salinity.

Regarding the W-E transect or TWE (66° to 75°E, along 47°S, Fig. 2 a,c,e), vertical cross sections of temperature and salinity with a T-S diagram are illustrated in Fig 2 (a,c,e). Temperature and salinity varied between 2.41° and 3.3°C, and between 33.60 and 34.67, respectively. A weak structure with colder and fresher surface waters was registered in the FP, which crossed these transects twice, at ~71°E (St. TWE03-04) and at ~73.5°E (StTWE07-08). Middle stations (Sts. TWE04, -05 and E) denoted an area with a complex recirculatory system in a stationary meander of the PF (Park et al., 2014), hereafter known as the Central Section. This section is superficial bathed by mixed Antarctic surface water (AASW) and coincides with the area with the PF northward inflexion (Fig. 1). The presence of Subantarctic mode water (SAMW) was observed east of 73.5° E (Sts. TWE07-08, Fig. 2f). In addition, a marked variability in subsurface water was observed, ascribed to mixing water masses; this was particularly strong in TWE within the PF, revealing a vertical mixing process produced by convergence, particularly evident at St. TWEO7 (Fig. 2e). Regarding the N-S transect (46°-51°S, along ~72°E) or TNS, Fig. 2 (b, d, f) shows vertical cross sections of temperature, salinity and a T-S diagram, respectively. Temperature and salinity fluctuated from 1.67° to 4.17°C and from 33.67 to 34.68, respectively, and a gradual decrease in temperature and an increase in salinity were observed in the surface layer from north to south (Fig 2 b, d). There was a water parcel of a relatively colder water mass spreading northward in subsurface waters. This was an expression of the PF, which marked the location where the AASW moving northward descended rapidly and sank below a depth of 200 m depth (Fig. 2

b). These distributions coincided with the expected water mass distribution, this being the case for the northern (Sts. TNS01-02) and southern (Sts. A3, TNS10) stations, mainly occupied from the surface to 250 m by the SAMW and the AASW, respectively (Fig 2f).

**3.2. Biogeochemical variables**

Figure 3 shows vertical cross sections along the TWE of biogeochemical variables including nutrients (only $NO_3^-$ and $HPO_4^{2-}$), T*Chl-a*, $O_2$ and GHGs. The surface layer continuously showed $NO_3^-$ concentrations, fluctuating from 22 to 27 µmol $L^{-1}$ (typical condition of the AASW). However, a relative depletion of $NO_3^-$ was observed at the stations located north- and eastward of the PF (Fig 3a). $PO_4^{3-}$ presented the same pattern as $NO_3^-$ and the N:P ratio of dissolved nutrients averaged around 14.5, with the exception of some values of 13.2 from stations located closed to the PF (Fig. 3 b). *TChl-a* fluctuated from 0.005 to 4.69 µg $L^{-1}$ and peaked at Sts. TWE01-02 (both located in a coastal area 10 and 75 km away from Hillsborough Bay coast) and Sts. TWE07-08 (to the north of PF). *TChl-a* showed a relative decrease at stations located in the Central Section (Fig. 3c). The observed pattern (Lasbleiz et al., 2014) significantly correlated with the dFe spatial distribution reported by Quéroué et al. (this volume). $O_2$ concentration varied form 320 µM (in surface water) to 185 µM (at 500 m deph), consistently maintaining super saturation conditions (Fig 3d).

$N_2O$ fluctuated from 14.0 to 25.4 nmol $L^{-1}$ (equivalent to a range of 102-182.2% saturation, Fig 3e). Superficially, the $N_2O$ concentration was close to equilibrium with the atmosphere in surface waters in the western and central section (70.5°- 73°E) and slightly undersaturated (around 90%) in surface waters in sites where the PF crosses the transect, i.e., Sts. TWE04 and TWE07 (Fig. 3e). $N_2O$ levels increased slightly attaining around 120% saturation towards subsurface water. $CH_4$ ranged from 1.4 to 31.35 nmol $L^{-1}$, equivalent to a range of saturation of 43-969%. In contrast to $N_2O$, surface waters were always supersaturated in $CH_4$, showing the highest increase in gas levels (up to 970%) in coastal waters

close to Kerguelen Island, a relative decrease (<200% saturation) in the central section (between 71° and 73.5°S, or Sts TWE04, 05 and E2), and a strong increase (up to 778%) at St, TWE07. Remarkably, $CH_4$ concentrations in subsurface waters were low compared to the surface waters (Fig. 3f).

Vertical cross sections of biogeochemical variables along the TNS are shown in Figure 4. $NO_3^-$ and $PO_3^{4-}$ gradually increased from north to south from 24 to 30 µmol $L^{-1}$ and from 1.5 to 2 µmol $L^{-1}$, respectively (Fig 4 a, b). This spatial trend coincided with the expected transition of water mass dominance and its mixing between the SAMW and the AASW (Fig 2 f). T*Chl-a* ranged from 0.005 to 2.391 µg $L^{-1}$ and peaked in the southernmost stations (Sts. TNS08, -09 and A3-2; Fig. 4b) and coincided with a slight increase in nutrients. These trends coincided with the presence of the central plateau area of the KPR, where upwelling-like circulation was observed (Zhou, this volume), as indicated by temperature and salinity distribution (Fig. 2 b, d). There a deep Fe-enriched and lithogenic silica reservoir seems to be influencing the area (Lasbleiz et al., 2014; Quéroué et al., 2014). $O_2$ distribution was similar to that observed in the WE transect.

$N_2O$ concentrations ranged from 12.37 to 23.8 nmol $L^{-1}$, equivalent to 88.5% to 171% saturation. $N_2O$ levels close to equilibrium or undersaturation were often observed in surface waters, except at St. TNS08 (Fig. 4e). $CH_4$ varied from 1.47 to 21.88 nM, or 45 to 666% saturation, and peaked in southern stations (Fig 4f). Notably, T*Chl-a* corresponded to the observed $CH_4$ in this transect. Southern stations, such as St. A3, located in an area of relatively high bioavailable Fe and within a phytoplankton bloom, had extremely low $N_2O$ concentrations (less than 6.9 nM or 70% saturation).

PCA, including dFe and GHG data were obtained from the TWE as shown in Figure 5. The results did not change when $O_2$ was removed from the analysis, indicating that this $O_2$ availability does not explain the variability. Using environmental data come from the ML (Fig. 5a), stations located on the TWE were grouped into three sets, clearly separating stations located on the eastern (north of the PF, St. TWE07),

the western or coastal area (TWE01-02), and Central section (Sts. TWE04, -05, E2). The variability among stations can be predominantly explained by the first component, accounting for 75.7% of the variance. Figure 5 demonstrates possible interpretations for relationships among the variables with their respective weights assigned to each of them (illustrated with an eigenvector). The figure shows a close relationship between $N_2O$, nutrients, $CH_4$, Fe and T*Chl-a*. The PCA analysis using data from the entire water column provided a similar grouping of the sample stations (Fig 5b).

**3.3. Vertical distribution of gases and other variables at selected stations**

Figure 6 shows typical profiles of oceanographic and biogeochemical variables (including gases). Stations were separated *a priori* according to biogeochemical (PCA analysis for the case of the TWE; Fig.5) and oceanographic criteria (T-S diagram, Fig. 2e, f). Selected stations included: Sts. A3, with a quasi-permanent phytoplankton bloom (historical station sampled in KEOPS 1, Blain et al., 2007) and low Fe levels (~ 0.18 nmol $L^{-1}$), but with the evidence n of an active uptake of dFe uptake; St. TWE07, which had moderate dFe (~0.40 nmol L-1) and high T*Chl-a* levels and also evidences of rapid dFe uptake (Fourquez et. this volume). For comparative purpose, we include the most northern station of the NST (St. TNS01), a well-known as a Fe-limited HNLC area (St. R), and a coastal station close to Kerguelen Island, which had the highest dFe levels (up to 3.82 nmol $L^{-1}$). Vertical distribution of $N_2O$ and $CH_4$ differed markedly, while elevated $CH_4$ concentrations were mostly located superficially and in the ML base and decreased as depth increased, $N_2O$ concentrations gradually increased with depth. Gas contents also differed between stations and were in similarly correlated with T*Chl-a* and dFe levels. Stations located in the extreme point of the WET (i.e., TWE01 and TWE07) had the highest $CH_4$ levels (Fig 6), while $N_2O$ levels were relatively low. On the other hand, Sts. TNS1 and A3, located in the extreme north and south of the N-S transect presented relatively low levels of $CH_4$ compared to the WET t. Station R, which is located in one of the more oligotrophic conditions of the Southern Ocean (special

volume of KEOPS 1), had the lowest $N_2O$ and $CH_4$ content, and both gases were homogeneously distributed with depth (Fig. 6). This is consistent with the expected trophic condition with T*Chl-a* levels of less than 0.5 µg $L^{-1}$**.**

### 3.4. Nutrient, T*Chl-a,* dFe and GHG inventories and air-sea GHG exchanges

Table 2 shows the inventories of $NO_3$, $PO_4^{3-}$ and GHGs in the ML and the water column from the surface to 500 m; mean GHG concentrations in the ML, wind speed and air-sea GHG fluxes are also included. ML depths varied widely from 16 m (at the station near Kerguelen Island) to 181 m. The T*Chl-a* pool, estimated on the basis of the photic layer, fluctuated from 8.77 to 75.45 mg $m^{-2}$. It was notably greater at Sts. SPF and A3-2 (up to fivefold greater) than at more oligotrophic stations like St. R. Surface $NO_3^-$ and $PO_4^{3-}$ inventories, which varied from 1.56 to 16.03 and 0.13 to 1.07 mol $m^{-2}$, respectively, did not show significant differences among stations. Minimal values were registered at stations St. TWE07-08 and TNS01, both located north of the PF.

$N_2O$ pools varied from 0.201 to 2.55 and from 1.12 to 10.05 mmol $m^{-2}$ in the ML and the whole water column, respectively. Minimum values were registered in the ML at stations within or north of the PF. These surface pools did not significantly correlate with T*Chl-a*, but correlated strongly and negatively with nutrients (rs: 0.91 $p<0.001$ for $NO_3^-$ and rs: 0.92, $p<0.001$ for $PO_4^{3-}$). $CH_4$ inventories fluctuated between 0.19 and 3.31 mmol $m^{-2}$ for the ML and 1.06 and 7.44 mmol $m^{-2}$ for the whole water columns. Once again, inventories in the ML were two and fivefold higher at Sts. TWE07 and A3-2, respectively, than at St. R. $CH_4$ inventories were four and sevenfold higher in Sts. TWE07 and A3-2 than at St. R. The comparison between the $CH_4$ inventories standardized by the thickness of the layer), obtained from the ML and from the entire water column, indicate that the maximum values came from the ML´s base, remarkably in the PF (Table 2). $CH_4$ pools correlated positively with T*Chl-a* pools (rs= 0.69; $p<0.05$),

but did not show any correlation with $NO_3$- and $PO_4^{3-}$. Thus, minimum values for both nutrients were found when T*Chl-a* was higher.

Average hourly wind velocity during the cruise was 10.53 ±5.52 m $s^{-1}$, occasionally falling below 0.31 m $s^{-1}$ or rising above 29.1 m $s^{-1}$. The ML depth did not show any significant relationship to wind speed (rs: 0.20 p=0.41) or the water mass structure (Table 1 and Fig. 2), but seems to be related to the complex mesoscale circulation observed in the KPR (Park et al., 2014; Zhou et al. this volume). $N_2O$ fluxes, estimated by LM86, fluctuated between -9.69 and 10.02 (mean: 1.25±4.04 µmol $m^{-2}$ $d^{-1}$), while those estimated by W92 varied from -18.69 to 20.2 µmol $m^{-2}$ $d^{-1}$ (mean: 2.41±7.88). At high wind speeds, such as those measured during the N-S transect (21-23 October 2011, mean value of 12.08 m $s^{-1}$) compared to those registered during the W-E transect (31 October – 02 November, mean value of 5.61 m $s^{-1}$), substantial differences were observed between the cubic (LM86) and the quadratic parameterizations (W92). The latter increased in calculated fluxes by approximately a factor of two at high wind speeds, while at low wind speeds the difference between LM86 and W92 was up to a factor of ~1.6 (see Table 2). $CH_4$ fluxes varied from 0.21 to 38.1 (mean: 10.01±9.97) and from 0.32 to 70.24 (mean: 21.27±21.07) µmol $m^{-2}$ $d^{-1}$, when LM86 and W92 were used, respectively. The study area at times acts as a source of very high $CH_4$ effluxes into the atmosphere, particularly at stations St. TNS09 and St. A3-3, where emissions were around three times as high as those calculated for St. R. There are important differences between the two parameterizations, although the same trend was obtained among stations (Table 2).

## 4. Discussion

### 4.1. Physical and geochemical characteristics

The Antarctic Polar Front (PF) marks an important climate boundary in terms of oceanic heat and salt budgets and a biogeochemical frontier with respect to GHG content and air-sea GHG fluxes (such as $N_2O$ and $CH_4$). The PF path exhibits considerable variability, meandering and forming eddies and rings. The location of the PF is mainly determined by the movements of deep waters and is probably strongly influenced by topography and bathymetric features such as the Drake Passage and the Kerguelen Plateau (Sandwell and Zhang, 1989; Patterson, 2005). These mesoscale structures in the study area are always associated with strong vertical and lateral mixing and advection (Park and Viver, 2012, Park et al., 2014; Zhou et al, this volume) that could create fertilization mechanisms (by both Fe and nutrient like silicate), therefore provoking *TChl-a* production which in turn is being stimulated by the addition dFe from different sources (Quéroué et al. this volume).

In some regions, the main Fe input is from atmospheric deposition (Jickells et al., 2005). However, this was not the case in the KPR. The main sources of iron that were evidenced in the KPR, that could also potentially fertilize the northern section of the plateau, were direct runoff from the Kerguelen Island, glacial melting and sedimentary inputs (Quéroué et al., 2014). Actually, the water masses found at stations north of the PF (e.g. TEW07) interacted more with the plateau and the shallow coastal waters of Kerguelen Island, than with the water masses from the recirculation area. This theory is consistent with the circulation data discussed by Park et al. (2014) who demonstrated that water masses are carried northwards between the island and the recirculation area and finally looped back east of the recirculation area.

The origin of the bloom in the central part of the plateau possibly comes from a deep Fe-enriched reservoir which was observed also above the Kerguelen Plateau during the KEOPS1 cruise (Blain et al., 2008; Chever et al., 2010). Non reductive dissolution of resuspended sediments is a potentially important source of dFe; at station A3, high lithogenic silice (LSi) concentrations ($1.34 \pm 0.07$ µmol $L^{-1}$;

Lasbleiz et al., 2014) were observed just above the seafloor in the benthic boundary layer (BBL), also suggesting sedimentary inputs. In fact, using Ra isotopes to trace Fe, Sanial et al. (2014) indicated that Fe could be supplied from sedimentary sources, as well as laterally advected from the southern region of Heard Island and exchanged through the Polar Front. Similar results were found during KEOPS 1 by Mongin et al. (2008), Zhang et al. (2008), and Maraldi et al. (2009).

Iron fertilization in the KPR has in influence on phytoplankton growth and primary production (PP), and other microbial activities (Cavagna et al., 2014; Christaki et al., 2014), as well as relative $CH_4$ accumulation (Fig. 3,f and Fig. 4f) and some $N_2O$ depletion (Fig 3e) were also observed. The gas distribution pattern clearly matched with TChl-a and PCA grouped stations as was made by Queroue et al (this volume) using dFe. The separation of stations comprises coastal area (Sts. TWE01, -02), the PF (St. STWE07) and central plateau region (Sts. A-3). In the case of KEOPS 2, phytoplanktonic blooms were mainly represented by a microplanktonic community (Lasbeiz et al, this volume) as those observed in the north Polar Front (St. TWE07) and the central part of the KPR (A3) stations displayed high rates of iron uptake (Quéroué et al, 2014). The mentioned areas, resented variable but high particulate Fe of biogenic origin (van der Merwe et al., 2014), confirming an increased biological uptake, which in turn determines a rapid dFe turnover. The observed gas distribution patterns raise questions as to how the complex circulation and some mesoscale structures support relatively high T*Chl-a* accumulation and microbial activities in comparison to surrounding waters, and particularly whether there are some fertilization mechanisms (including the addition Fe and nutrients) promoting GHG cycling and the concomitant microbial activities.

### 4.2. $N_2O$ cycling

Fuhrman and Capone (1991) pointed out that stimulating ocean productivity by Fe addition, which enhances nitrogen export from the euphotic zone to the subsurface layer, can result in enhanced $N_2O$

formation via stimulated nitrification. This stimulation could occur through the activation of metallo-proteins that are involved in various steps of ammonium and nitrite oxidation, as ammonia oxidizing nitrifiers use iron-containing ammonia monooxygenase (AMO) and hydroxylamine oxidoreductase (HAO) to oxidize $NH_4^+$ and $NH_2OH$, respectively, to $NO_2^-$ (Morel et al, 2003b). Since $N_2O$ is a powerful greenhouse gas, 300 times more radiative than $CO_2$ per molecule, Fe addition could counteract the climatic benefits of atmospheric $CO_2$ drawdown (Jain et al., 2000). The link between Fe fertilization and enhanced $N_2O$ formation via nitrification was supported by Law and Ling (2001), who found a small but significant $N_2O$ accumulation in the pycnocline during the Southern Ocean Iron Enrichment Experiment (SOIREE) at 61°S, 140°E. Jin and Gruber (2003) subsequently predicted the long-term effect of Fe fertilization on global oceanic $N_2O$ emissions using a coupled physical-biogeochemical model. Based on the model outputs, they concluded that Fe fertilization induced $N_2O$ emissions that could offset the radiative benefits of the $CO_2$ drawdown. However, during other Southern Ocean Iron Enrichment Experiments (EIFEX), Walter et al. (2005) found no $N_2O$ enrichment after artificial Fe fertilization.

Our findings revealed that natural Fe fertilization did not seem to stimulate $N_2O$ accumulation superficially (within the ML). The $N_2O$ inventory estimates from areas of higher accumulation of biomass were not significantly different with respect to those estimated for St. R, which was used as a reference station (Table 2). Contrary to what was expected, no increase in $N_2O$ content was observed at stations close to Kerguelen Island (St TWE01, TWE02), which are highly enriched by dFe from fresh water and sediments (Quéroué et al., this volume). This trend suggests that nitrifiers in surface water are not being significantly stimulated by Fe supply from the sediments. At subsurface water (below ML to 500 m depth) $N_2O$ accumulation may be associated to nitrification In fact, dual nitrate isotopic composition ($\delta\ ^{15}N\text{-}NO_3^-$ and $\delta\ ^{18}O\text{-}\ NO_3^-$) revealed an increasing of values for both isotope values as water

depth increase in subsurface waters (100–400 m) as being the result of partial consumption of available nitrate in surface waters, export of low $\delta\ ^{15}N$ in Particulate Nitrogen (NP) and remineralisation–nitrification there (Dehairs et al., 2014) Although, values of $\delta\ ^{15}N\text{-}NO_3^-$ and $\delta\ ^{18}O\text{-}\ NO_3^-$ in surface water also suggested that nitrification is also occurring in surface water, but with a considerable variation

Remarkably, the St. TW07-08 and A2-3 were in equilibrium and slightly depleted in $N_2O$ (Fig. 3e; Table 2). The only plausible explanation is that mixing process produced at the PF (St. TWE07) (which have moderate Fe levels, high T*Chl-a* and evidence of active Fe uptake) may stimulate the N fixers, as demonstrated by Mills et al. (2004), Berman-Frank et al. (2007), and Moore et al. (2009). N-fixing microorganisms may have an effect on the $N_2O$ inventory as they could be used as an alternate substrate for fixers, as suggested by Farias et al. (2013). Thus, biological $N_2O$ fixation could be using and assimilating $N_2O$, producing $N_2O$ depletion and a concomitant undersaturation. N-fixation has been observed in the cold waters of the Arctic and Antarctic (Blais et al., 2012; Diez et al., 2012, Diez unpublished data), as well as in cold upwelled water (Fernandez et al., 2011), suggesting that $N_2O$ fixation may also be action and it is a well-spreading process than originally expected. Coincidently, St. SPF also had the highest surface N-fixation (Gonzalez et al. this volume), suggesting that $N_2O$ is used as a substrate by diazotrophs (Farias et al., 2013) and that this process is stimulated by enhanced Fe supply. $N_2O$ undersaturation or equilibrium with the atmosphere was observed in the N-S transect (Fig, 4e), particularly at stations north of the PF bathed by SAMW. This suggests that some process is removing or consuming this gas in the upper water column. A notable level of undersaturation was also observed at St. A3-2, which is located in the recurring phytoplankton bloom and in a regime of relatively high dFe concentration due to the presence of the Plateau (Blain et al., 2007).

$N_2O$ undersaturation has been reported, although rarely, in Polar and Sub-polar Ocean regions (Butler et al., 1989; Law and Ling, 2001; Foster et al., 2009). Physical processes related with gas solubility and

deviations of from atmospheric equilibrium gas concentration could not explain the observed undersaturation. If these physical variables change in less time than that required for equilibrium of the gases with the atmosphere, there may be a gas deficit. Thus, deviation from the equilibrium condition could be caused by rapid heating or cooling, refreshing, and/or a mixing of water masses (Sarmiento and Gruber, 2006). An analysis of these potential changes was made for the AASW and the SAMW. A cooling (decreasing T°C> 3) or freshening processes (decreasing S from 34 to 10) are required to produce the observed undersaturation, neither of which was observed during the sampling (Table 1), or expected during this season (Park and Viver, 2012). Additionally, if the two water masses were mixed proportionally, as they are, the resulting process cannot produce undersaturation regarding the original $N_2O$ levels and their temperature and salinity signature. Recently, Chen et al. (2014) reported that surface water of the Southern Ocean of Indian sector were understaturated in $N_2O$, reflecting also a $N_2O$ influx. This phenomenon in the surface water may result from ice melt water intrusion and northeastward transport of the AASW. However, in the KPR, $N_2O$ undersaturation seems to be located in area of high particle concentration under the influence if in the SAMW (northern the PF), Thus, a preliminary analysis indicates that biological processes are responsible for the $N_2O$ undersaturation and the concomitant influx from the atmosphere. In contrast, subsurface waters have higher $N_2O$ concentrations (saturations from 120% to 180%) than surface waters, which indicate a net accumulation. In this case the plausible process responsible for $N_2O$ accumulation is aerobic ammonium oxidation (Codispoti et al., 2001), but no significant difference was noted at the stations with the highest T*Chl-a* levels, indicating that $N_2O$ production by nitrification was not substantially stimulated at those stations.

### 4.3. $CH_4$ cycling

There have been few studies on $CH_4$ distribution and production in the Southern Ocean (Lamontage et al., 1973; Tilbrook and Karl, 1994; Heeschen et al., 2004). There, surface water has been reported to be undesaturated or lightly saturated with respect to atmospheric $CH_4$, as the result from the entrainment of $CH_4$ depleted deep water into surface water and from the seasonal ice cover acting as a barrier for gas exchange (Toshida et al., 2011). Regarding the effect of iron addition on $CH_4$ cycling Wingenter et al. (2004) found low levels of $CH_4$ production (less than 1%) during artificial Southern Ocean Fe enrichment experiments (SOFex). Simulated large-scale Southern Ocean Fe fertilization (OIF) also resulted in anoxic conditions which may favor anaerobic methanogenesis (Oschlies et al. 2010). However, our results show that surface and subsurface water are supersaturated in $CH_4$ with a fourfold enrichment in $CH_4$ with respect to the control area (Fig. 3e), this was associated to areas with elevated T*Chl-a* levels and iron uptake by microbial communities (Fourquez et al., 2014).). Results showed marked spatial differences in $CH_4$ content measured in the W-E and N-S transect (t-student: 3.21 $p<0.001$) (Fig. 3f and 4f), and that surface $CH_4$ accumulation generally coincided with areas of relatively higher dFe levels, which in turn favors primary production (PP). Likewise, the $CH_4$ accumulation at pycnoclines (Fig. 6) indicates that most $CH_4$ came from accumulated particles sinking from the surface water, as commonly observed by Holmes et al. (2000) in different marine systems. The PCA analysis, which included the measurement of dFe revealed a close relationship between $CH_4$ accumulation and Fe availability and clearly grouped in areas with different biogeochemical characteristics. The fact that the western and eastern sections showed high Fe levels (Quéroué, this volume) relative to the Central Section of the W-E transect, and that these sections had high $CH_4$ levels, suggests that Fe in some way stimulates $CH_4$ production. A similar situation occurs in Sts.A3 with high T*Chl-a* levels and PP rates, as shown by Cavagna et al. (2014). For example, station A3-2 and TWE07 (maximum T*Chl-a*) had the

highest integrated primary production rates (up to 3380 mg $m^{-2}$ $d^{-1}$) and the lowest C export level of around 2-3% (Cavagna et al., 2014), this suggests an intense level of PP supported by regenerated N sources. These contrast with condition found at St. R with the lowest rate of regenerated production (with a PP rate of around 135 mg $m^{-3}$ $d^{-1}$ and an exported C rate of around 25% of PP).

Two hypotheses exist about $CH_4$ production in surface waters. One is that it should only occur in association with anoxic particles (Karl and Tilbrook, 1994) most of them being produced by grazing zooplankton, as methanogenic bacteria were considered to be present in an anaerobic microenvironment in organic particles (pellets) or in the guts of zooplankton (Alldredge and Cohen, 1987; Karl and Tilbrook, 1994)The other hypothesis was formulated more recently, that that phytoplankton blooms should favor zooplankton grazing process and/or stimulate bacterioplankton activity as $CH_4$ is generated via the degradation of organic methyl compounds by bacteria (Karl et al 2008).

Increased grazing of microbes by microzooplankton, as observed by Christaki et al. (2014) and may contribute to particle recycling (rich in organic carbon and DMSP), and increase the potential for methanogenesis (Weller et al., 2013). Yoshida et al. (2011) found that high $CH_4$ production in the Southern Ocean probably resulted from the grazing processes of Antarctic krill and/or zooplankton fed on phytoplankton, and the subsequent microbial methanogenesis. This was in line with the findings of iron and biomass enriched sites exhibited the highest carbon fluxes at 100 m depth, mainly dominated by large fecal pellets, rather than phytodetrital aggregates (Laurenceau et al., 2014).

On the other hand, aerobic $CH_4$ production in the water column could be associated with heterotrophic activities. Christaki et al. (2014) showed that the highest bacterial production rates (up to 110 mg C $m^{-2}$ $d^{-1}$), and the greatest abundance of heterotrophic bacteria were associated with stations where the phytoplankton bloom was developed (TWE07 and A3-2). Recent evidences indicate that methylotrophs are candidates for mediated $CH_4$ generation using methylated compounds as DMSP and DMS (Florez-

Leiva et al., 2013; Weller et al., 2013). Among these heterotrophic microorganisms DMS degradation can be ascribed to methylotrophic bacteria (Vissher et al., 1994) that derive energy from the conversion of methyl into other products, as well as using S as a source for methionine biosynthesis (Kiene et al., 1999). Current studies of natural and cultivated SAR11 alphaproteobacteria (strain Ca. P. ubique HTCC1062; Sun et al., 2011) indicate that these microorganisms, among the most abundant heterotrophic bacteria in surface waters, possess genes that encode for oxidation pathways of a variety of one-carbon compounds, and have the capacity for demethylation and C1 oxidation, but do not incorporate C1 compounds as biomass. These facts suggest a close relationship between phytoplankton, the only producers of DMSP (Yoch, 2002), and microbial communities which may be recycling DMS. Phyto- and bacterioplankton relationships control DMS turnover, which could result in several mechanisms of DMSP/DMS degradation (Simó et al., 2002; Vila-Costa et al., 2006) and produce $CH_4$ (Damm et al., 2010; Florez-Leiva et al., 2013; Weller et al., 2013). These authors showed that phytoplankton species composition and biomass in different bloom phases, as well as eddy dynamics, were important determinants of $CH_4$ saturation and emission.

Regarding vertical distribution of this gas, profiles indicate that most $CH_4$ is being formed at the surface and at pycnoclines (at the base of the ML), and consumed at subsurface and intermediary depths (Figure 6). Thus, $CH_4$ distribution appears to be controlled largely by biological mechanisms rather than by mixing, contrary to what has been reported by Heeschen et al., (2004). In general, surface waters of the Southern Ocean were undesaturated with respect to atmospheric $CH_4$ as the result of the entrainment of $CH_4$ depleted deep water to the surface and from seasonal ice cover acting as a barrier for gas exchange. We observed $CH_4$ undersaturation, fluctuating between 40% and 90%, at most sampled stations at depths of > 200. It is unlikely that undersaturation results from the entrainment of $CH_4$-depleted waters that have high levels of gas solubility, but also by a biological consumption. It is more likely that a

biological mechanism is involved. The only known process able to consume $CH_4$ is methanotrophy, and the fact that subsurface waters were depleted of $CH_4$ suggests that $CH_4$ consumption is higher than production, or that no production occurs in subsurface waters. Interestingly, although $CH_4$ microbial oxidation occurs throughout the water column and is recognized as an important process that reduces $CH_4$ emissions (Reeburgh et al., 2007; Rehder et al., 1999), microbial communities mediating aerobic $CH_4$ oxidation have scarcely been investigated. There have been few measurements of aerobic $CH_4$ oxidation in marine environments, and measurements taken from open systems under oligotrophic regimes (Tilbrook and Karl, 1994, Holmes et al., 2000) have found lower levels of oxidation than in the oxic/anoxic interface (Sansone and Martens, 1978 Reeburgh et al., 1991).

### 4.4. $CH_4$ and $N_2O$ emission in the southern Ocean

Highly dynamic gas exchanges were registered in the KPR, with source and sink scenarios for $N_2O$ and just a source scenario for $CH_4$. Since the mean wind speed did not exceed 14 m $s^{-1}$, LM86 and W92 parameterizations represent the more conservative overestimation estimates of gas exchange in the area (Frost and Upstill-Goddard, 2003). The gas inventories in the ML reflect the effect of gas transport mainly via turbulent mixing and advection, which can be accelerated by the action of wind but also by the microbial activity in surface waters. The ML depth did not correlate to wind speed (rs: 0.31, $p < 0.05$). This fact would explain how much of the content of the gases in the ML may come from in situ production or consumption. $CH_4$ fluxes were higher at stations located at the PF and A3, where phytoplaktonic blooms were observed (see Table 2), but the tendency was the reverse for $N_2O$, with an influx into the aforementioned stations. $CH_4$ emission rates during this study were higher than previous measurements (Table 2), with a range of 0.1 to 3.0 μmol $m^{-2}$ $d^{-1}$ for the Pacific Ocean (Bates et al., 1996; Holmes et al., 2000; Sansone et al., 2001) and 0.5 to 9.7 μmol $m^{-2}$ $d^{-1}$ for the Atlantic Ocean

(Oudot et al., 2002; Forster et al., 2009). In the South Pacific ocean (10°-64°S, 140°E), crossing the PF, Yoshida et al. (2011) reported $CH_4$ fluxes ranging from 2.4 to 4.9 μmol $m^{-2}$ $d^{-1}$.

In the case of $N_2O$, the estimates in this study were in the expected range for the oligotrophic open ocean (Nevinson et al., 1995). $N_2O$ undersaturation and a concomitant influx were estimated, although this situation has not yet been well described for the Southern Ocean. $N_2O$ sinks can occasionally be observed (Butler et al., 1989; Law and Ling, 2001), the most plausible explanation for which is $N_2O$ assimilation by N-fixing microorganisms. This process may be responsible for the estimated $N_2O$ influx.

## 5. Implications

The dynamics of the both gases differ substantially both spatially and vertically (surface to 500m depth), indicating that different mechanisms are being activated producing an active gas during recycling. Our findings also show that in areas of active fertilization and biogenic particle accumulation, $CH_4$ accumulates while $N_2O$ becomes depleted. This study suggests that the Antarctic Polar Zone plays a significant role in surface $CH_4$ production and subsequent air-sea gas exchange. These results did not agree with some previous studies of artificial fertilization experiments in the Southern Ocean, even though only a few previous studies exist, indicating that the turnover and evolution of microbial communities in mesoescale structure are fundamental for the development of substrates and conditions for $CH_4$ regeneration. Surface $N_2O$ does not spatially respond to natural stimulation, at least in terms of $N_2O$ production via nitrification or that $N_2O$ consuming are faster than $N_2O$ producing process, but in subsurface water $N_2O$ accumulation seems to take place via nitrification).

**Acknowledgements**: We would like to thank the captain and crew of the R/V Marion Dufresne. We recognized the support of INSU/LEFE/Cyber and ANR for supporting KEOPS2 and also both project

leaders (Stephane Blain and Bernard Queguiner) We are also grateful to Louise Oriol and Stephane Blain for nutrient data and Marine Lasbleiz for the HPLC analysis of chlorophyll measurements. We also recognize all our colleagues that contributed to KEOPS 2. CF and LF were supported by the Proyecto Ecos-Conicyt C09B02 and the International Associated Laboratory MORFUN. CF received partial support from Fondap N°15110027. LF founded the analysis of samples obtained in the KEOPS 2 cruise with FONDECYT N° 1120719. This is a contribution by 15110009 (FONDAP-CONICYT).

## References

Alldredge, A. L. and Y. Cohen. Can microscale chemical patches persist in the sea? Microelectrode study of marine snow, fecal pellets, Science, 235, 689–691, doi:10.1126/science.235.4789.689, 1987.

Arrieta, J.M., Weinbauer, M.G., Lute, C. and Hernd, G.J. Response of bacterioplankton to iron fertilization in the Southern Ocean, Limnology and Oceanography, 49(3), 799-808, 2004.

Bates T.B., Kelly, K.C., Johnson, J.E. and Gammon, R.H. A re-evaluation of the open ocean source of methane to the atmosphere, Journal of Geophysical Research, 101 (D3), 6953–6961, 1996.

Berman-Frank, I., Quigg, A., Finkel Z. V., Irwin A.J., Haramaty, L. Nitrogen-fixation strategies and Fe requirements in cyanobacteria, Limnology and Oceanography, 52(5), 2260–2269, 2007.

Blain, S., Quéguiner, B., Armand, L., Belviso, S., Bombled, B., Bopp, L.,Bowie, A., Brunet, C., Brussaard, K., Carlotti, F., Christaki, U., Corbiére, A., Durand, I., Ebersbach, F., Fuda, J.L., Garcia, N., Gerringa, L.J.A., Griffiths, F.B., Guigue, C., Guillerm, C., Jacquet, S., Jeandel, C., Laan, P., Lefe`vre, D., Lomonaco, C., Malits, A., Mosseri, J., Obernosterer, I., Park, Y.H., Picheral, M., Pondaven, P., Remenyi, T., Sandroni, V., Sarthou, G., Savoye, N., Scouarnec, L., Souhault, M., Thuillers, D., Timmermans, K.R., Trull, T., Uitz, J., Van-Beek, P., Veldhuis, M.J.W., Vincent, D., Viollier, E., Vong, L and Wagener, T. Effect of natural iron fertilization on carbon sequestration in the Southern Ocean, Nature, 446 (7139), 1070–1075, 2007.

Blain, S., Sarthou, G. and Laan, P. Distribution of dissolved iron during the natural iron fertilization experiment KEOPS (Kerguelen Plateau, Southern Ocean), Deep-Sea Research II, doi:10.1016/ j.dsr2.2007.12.028, 2008.

Blain, S., Oriol, L., Capparos, J., Gueneugués, A., and Obernosterer, I. Distribution and stoechoimetry of dissolved nitrogen and phosphorus in the iron fertilized region near Kerguelen (Southern Ocean), Biogeosciences discussion KEOPS 2 special issue, 2014.

Blais, M.,Tremblay J.-É., Jungblut, A. D., Gagnon, J., Martin, J., Thaler, M. and Lovejoy, C. Nitrogen fixation and identification of potential diazotrophs in the Canadian Arctic. Global Biogeochemical Cycles, 26, GB3022, doi:10.1029/2011GB004096, 2012

Butler, J. H., Elkins, J.W., Thompson, T. M and Egan. K.B. Tropospheric and Dissolved $N_2O$ of the West Pacific and East Indian Oceans During the El Niño Southern Oscillation Event of 1987, Journal of Geophysical Research, 94, 14865-14877, 1989.

Cavagna, A.J., Lefèvre, D., Dehairs, F., Elskens, M., Fripiat, F., Closset, I., Laslbleiz, M., Florez-Leiva, L., Cardinal,D., Leblanc,K. , Fernandez, C, Oriol, L., Blain, S. and Quéguiner, B. Production regime and potential for carbon export in the naturally iron fertilized Kerguelen area (Southern Ocean). Biological productivity regime in the surface water around the Kerguelen Island in the Southern Ocean – from the use of an integrative approach. Biogeosciences discussion KEOPS 2 special issue, 2014.

Chen. L., Zhang, J., Zhan, L., Li, Y., Sun, H. Differences in nitrous oxide distribution patterns between the Bering Sea basin and Indian Sector of the Southern Ocean. Acta Oceanologica 33, . 9‑19, DOI: 10.1007/s13131-014-0484-8, 2014.

Chever, F., Sarthou, G., Bucciarelli, E., Blain, S. and Bowie, A.R.. An iron budget during the natural iron fertilisation experiment KEOPS (Kerguelen Islands, Southern Ocean). Biogeosciences, 7: 455-468, 2010.

Christaki, U., Lefèvre, D., Georges, C., Colombet, J., Catala, P., Courties, C., Sime-Ngando, T., Blain, S. and Obernosterer, I. Microbial food web dynamics during spring phytoplankton blooms in the naturally iron-fertilized Kerguelen area (Southern Ocean), Biogeosciences Discuss, 11, 6985–7028, doi:10.5194/bgd-11-6985-2014, 2014.

Cicerone, R.J. and Oremland, R.S. Biogeochemical aspects of atmospheric methane, Global Biogeochemical Cycles, 2, 299–327, 1988.

Codispoti, L.A and Christensen, J.P. Nitrification, denitrification and nitrous oxide cycling in the eastern Tropical South Pacific Ocean, Marine Chemistry, 16, 277-300, 1985.

Codispoti, L. A., Brandes, J. A. Christensen, J. P. Devol, A.H. Naqvi, S.W.A., Paerl, H.and Yoshinari, T. The oceanic fixed nitrogen and nitrous oxide budgets: Moving targets as we enter the anthropocene?, Scientia Marina, 65, 85-105, 2001.

Damm, E., Helmke, E., Thoms, S., Schauer, U., Nöthing, E., Bakker, K., Kiene, R.P. Methane production in aerobic oligotrophic surface water in the central Artic ocean, Biogeosciences, 7, 1099-1108, 2010.

Dehairs, F, Fripiat, F. , Cavagna A.-J. Trull, T. W. Fernandez, C., Davies, , D. Roukaerts A. , Fonseca Batista, D. Planchon, F. and Elskens M. Nitrogen cycling in the Southern Ocean Kerguelen Plateau area: evidence for significant surface nitrification from nitrate isotopic compositions Biogeosciences Discussion , 11, 13905-13955, 2014

Díez, B., Bergman, B., Pedrós-Alió, C., Antó, M. and Snoeijs P. High cyanobacterial nifH gene diversity in Arctic seawater and sea ice brine. Environmental Microbiology Reports 4, 360–366, doi:10.1111/j.1758-2229.2012.00343.x, 2012.

d'Ovidio, F., Zhou, M., Park, Y. H., Nencioli, F., Resplandy, L., Doglioli, A., Petrenko, A., Blain, S., and Queguiner, B.: Guiding biogeochemical campaigns with high resolution altimetry: waiting for the SWOT mission, Proceedings of 20 Years of Progress in Radar. Altimetry Symposium, Venice, Italy, 2012.

Emery, W.J and Thomson, R.E. Data analysis methods in physical oceanography, Pergamon Press, 634 pp, 1997.

Farias, L., Fernández, C., Faúndez, J., Cornejo, M. and Alcaman, M.E. Chemolithoautotrophic production mediating the cycling of the greenhouses gases $N_2O$ and $CH_4$ in an upwelling ecosystem, Biogeosciences, 6, 3053-3069, 2009.

Farias, L., Faundez, J., Fernadez, C., Cornejo, M., Sanhueza, S and Carrasco, C. Biological $N_2O$ fixation in the eastern South Pacific ocean, PLoS One 8, e63956, doi:10.1371 /journal.pome0063956, 2013.

Florez-Leiva, L., Damm, E. and Farías, L. Methane production induced by methylsulfide in surface water of an upwelling ecosystem, Progress in Oceanography, doi.org/10.1016/ j.pocean. 2013.03.005, 2013.

Fourquez, M., Obernosterer, I., Davies, D.M., Trull, T.W and Blain, S. Microbial iron uptake in the naturally fertilized waters in the vicinity of Kerguelen Islands: phytoplankton-bacteria interactions. Biogeosciences Discuss., 11, 15053-15086, 2014.

Frost, T., and Upstill-Goddard, R.C. Meteorological controls of gas exchange at a small English lake, Limnology and Oceanography, 47(4), 2002, 1165–1174, 2002.

Forster, G., Upstill-Goddard, R.C., Gist, N., Robinson, C., Uher, G.,Woodward, E.M. Nitrous oxide and methane in the Atlantic Ocean between 50°N and 52°S: Latitudinal distribution and sea--air flux, Deep-Sea Research II 56, 964-976, 2009.

Fuhrman, J.A. and Capone, D.G. Possible biogeochemical consequences of ocean fertilization, Limnology and Oceanography, 36, 1951-1959, 1991.

Grasshoff, J. Methods of seawater analysis. In: Grasshoff K, Ehrhardt M, Kremling K (eds.). Methods of seawater analysis Verlag chimie Germany, 1983.

Gonzalez, M.L., Molina, V., Florez-Leiva, L. Cavagna, A.J., Dehairs, F., Farias, L. and Fernandez, C. Nitrogen fixation in the southern ocean: A case of study of the Fe-fertilized Kerguelen region (KEOPS II cruise) Biogeoscience discussion bg-2014-576.

Hanson, R.S. and Hanson, T.E. Methanotrophic bacteria, Microbiology and Molecular Biology Reviews, 60(2), 439-471, 1996.

Heeschen, U. K., Keir, R. S., Rehder, G., Klatt, O and Suess, E. Methane dynamics in the Weddel Sea determined via stable isotope ratios and CFC‐11, Global Biogeochemical. Cycles, 18, GB2012, doi:10.1029/2003GB002151, 2004,

Holmes, R.H., Aminot, A., Kérouel, R., Hooker, B.A., Peterson, J. A simple and precise method for measuring ammonium in marine and freshwater ecosystems, Canadian Fisheries and Aquatic Sciences, 56,1801-1808, 1999.

Holmes, M.E., Sansone, F.J., Rust, T.M. and Popp, B.N. Methane production, consumption, and air-sea exchange in the open ocean: An evaluation based on carbon isotopic ratios, Global Biogeochemical Cycles, 14, 1 – 10, 2000.

IPCC. Climate Change: The Physical Science Basis: Working Group I Contribution to the Fourth Assessment Report of the IPCC (Climate Change 2007), M. Tignor and H.L. Miller [eds.]. Cambridge University Press, 2007.

Jain, A. K., Briegleb, B.P., Minschwaner, K. and Wuebbles D. J. Radiative forcing and global warming potentials of greenhouse gases, Journal Geophysical Research, 105, 20,773–20,790., 2000.

Jin, X. and Gruber, N. Offsetting the radiative benefit of ocean iron fertilization by enhancing $N_2O$ emissions. Journal Geophysical Research, 30, , 2249, doi:10.1029/2003GL018458, 2003.

Jickells, T. D., An, Z. S., Andersen, K. K., Baker, A. R., Bergametti, G., Brooks, N., Cao, J. J., Boyd, P. W., Duce, R. A., Hunter, K. A., Kawahata, H., Kubilay, N., laRoche, J., Liss, P. S., Mahowald, N., Prospero, J. M., Ridgwell, A. J., Tegen, I., and Torres, R.: Global iron connections between desert dust, ocean biogeochemistry, and climate, Science, 308, 67-71, 2005.

Jouandet, M-P., Jackson, G. A., Carlotti, F. , Picheral, M.,Stemmann, L. and Blain, S. Rapid formation of large aggregates during the spring bloom of Kerguelen Island: observations and model comparisons Biogeosciences Discussion., 11, 4949–4993, doi:10.5194/bgd-11-4949-2014, 2014.

Karl, D.M., Tilbrook, B.D. Production and transport of methane in oceanic particulate matter, Nature, 368, 732–734, 1994.

Karl, D., Beversdorf, L., Björkman, K.M., Church, M.J., Martinez, A., DeLong, E.F. Aerobic production of methane in the sea, Nature Geoscience, 1, 473-478, 2008.

Kiene, R.P. Linn, L.J. J. Gonzalez,J. M.A. Moran, M.A Bruton, J.A. Dimethylsulfoniopropionate and methanethiol are important precursors of methionine and protein-sulfur in marine bacterioplankton. Applied and Environmental Microbiology, 65 (10),4549–4558, 1999.

Kirchman, D.I, Hoffman, K.A. Weaver, R. and Hutchins, D.A. Regulation of growth and energetics of a marine bacterium by nitrogen source and iron availability, Marine Ecology Progress Series, 250, 291-296, 2003.

Lamontagne, R., Swinnerton, J. W., Linnenbom, V.J. and and Smith, W. D. Methane concentrations in various marine environments. Journal of Geophysical Research, 78, 5317-5324, 1973.

Laurenceau, E.C., Trull, T. W. , Davies, D. M. , Bray, S. G. , Doran, J. , Planchon F. , Carlotti, F. , Jouandet, M.-P., Cavagna, A.-J. , Waite, A. M. and Blain S. The relative importance of phytoplankton aggregates and zooplankton fecal pellets to carbon export: insights from free-drifting sediment trap deployments in naturally iron-fertilised waters near the Kerguelen plateau. Biogeosciences Discussion , 11, 13623-13673, 2014.

Law, C. and Ling, R. Nitrous oxide flux and response to increased iron availability in the Antarctic Circumpolar Current, Deep Sea Research Part II: Topical Studies in Oceanography, 48, 2509-2527, 2001.

Lasbleiz, M., Leblanc, K., Blain, S., Ras, J., Cornet-Barthaux, V., Nunige, S.H. and Quéguiner, B., 2014a. Pigments, elemental composition (C, N, P, Si) and stoichiometry of particulate matter, in the naturally iron fertilized region of Kerguelen in the Southern Ocean. Biogeosciences Discussion, 11: 8259–8324, 2014.

Liss P.S, Merlivat L. Air-sea gas exchange rates: Introduction and synthesis. In: Buat-Menard P. (ed.), The Role of Air-Sea Exchange in Geochemical Cycling. D. Reidel, Dordrecht, pp. 113-127, 1986.

Nevison, C., Weiss, R. and Erickson III, D.J. Global oceanic emissions of nitrous oxide, Journal of Geophysical Research, 100, 15809-15820,1995.

Nevison, C., Butler, J.H. and Elkins, J.W. Global distribution of $N_2O$ and the DN2O-AOU yield in the subsurface ocean, Global Biogeochemical Cycles, 7 (4), 1119, doi:10.1029/2003GB002068, 2003.

Maraldi, C., Mongin, M., Coleman, R.S. and Testut, L. The influence of lateral mixing on a phytoplankton bloom: distribution in the Kerguelen Plateau region. Deep Sea Research Part I, 56: 963-97, 2009.

Mills, M.M.,Ridame, C., Davey, M., La Roche, J and Geider, R. Iron and phosphorus co-limit nitrogen fixation in the eastern tropical North Atlantic, Nature., 429, 292–294, 2004.

Mongin, M., Molina, E. and Trull, T. Seasonality and scale of the Kerguelen plateau phytoplankton bloom: A remote sensing and modeling analysis of the influence of natural iron fertilization in the Southern Ocean, Deep Sea Research Part II: Topical Studies in Oceanography, 55(5-7), 880-892, 2008.

Moore, C.M , Mills, M.M., Achterberg, E.P., Geider., R J. LaRoche, J., Lucas, MI., McDonagh, E.L., Pan, X., Poulton, A.J., Rijkenberg, M J. A., Suggett, D.J., Ussher, S. J. and Woodward, E.M.S. Large-scale distribution of Atlantic nitrogen fixation controlled by iron availability, Nature Geoscience, 2, 867–871, 2009.

Morel, F.M.M. and Price, N.M. The biogeochemical cycles of trace metals in the Oceans, Science, 300, 944, DOI: 10.1126/science.1083545, 2003a.

Morel, F. M. M., Milligan, A.J. and Saito M.A.. Marine Bioinorganic Chemistry: The Role of Trace of Metals in the Oceanic Cycles of Major Nutrients in *Treatise on Geochemistry*, Vol. 6, edited by KK. Turekian, H.D. Holland, Elsevier Science Ltd, Cambridge, UK, p. 113-143, 2003b

Oudot, C., Jean-Baptiste, P., E. Fourreb, E. Mormichea, C. Guevela, M., Ternonc, J.-F , Le Corred, P. Transatlantic equatorial distribution of nitrous oxide and methane, Deep-Sea Research I, 49,1175–1193, 2002.

Oschlies, A., W. Koeve W., Rickels W., and Rehdanz, K. Side effects and accounting aspects of hypothetical large-scale Southern Ocean iron fertilization, Biogeosciences 7, 4017–4035, 2010.

Park, Y-H and Viver, F. Circulation and hydrography over the Kerguelen Plateau. Marine ecosystems and fisheries, 5, 43-55, 2012.

Park, Y.-H., Durand, I., Kestenare, E., Rougier, G., Zhou, M., d'Ovidio, F., Cotté, C. and Lee, J.-H. Polar Front around the Kerguelen Islands: An up-to-date determination and associated circulation of surface/subsurface waters. Journal Geophysical Research- Oceans, 119: doi:10.1002/2014JC010061, 2014.

Patterson, S L. Surface Circulation and Kinetic Energy Distributions in the Southern Hemisphere Oceans from FGGE Drifting Buoys, Journal of Physical Oceanography, 15, 865–884, 2005.

Quéroué, F., Sarthou, G., Chever, F., van der Merwe, P., Lannuzel, D., Townsend, A.,Bucciarelli, E, Planquette, H., Cheize, M., Blain, d'Ovidio, F. and A. Bowie, A. A new study of natural Fe fertilization processes in the 2 vicinity of the Kerguelen Islands (KEOPS 2 experiment), KEOPS 2 special issue (in preparation).

Rees, A.P., Owens, N.J.P and Upstill-Goddard, R.C. Nitrous oxide in the Bellingshausen Sea and Drake Passage, Journal of Geophysical Research,102, 3383– 3391, 1999.

Reeburgh, W.S, Ward, B.B, Whalen, S.C., Sandbeck, K.A., Kilpatrick, L.J and Kerkhof, K. Black Sea methane geochemistry, Deep-Sea Research II (38) S1189–S1210, 1991.

Reeburgh, W.S. Oceanic methane biogeochemistry, Chemical Reviews 107, 486–513, 2007.

Rehder, G., Keir, R.S., Suess, E., Rhein, M. Methane in the northern Atlantic controlled by microbial oxidation and atmospheric history, Geophysical Research Letters 26, 587–590, 1999.

Rhee, T. S., Kettle, A. J and Andreae, M. O. Methane and nitrous oxide emissions from the ocean: A reassessment using basin-wide observations in the Atlantic, Journal of Geophysical Research, 114,D12304, doi:10.1029/2008JD011662, 2009.

Sanial, V., van Beek, P., Lansard, B., Souhaut, M., Kestenare, E., and d'Ovidio, F.: Radium isotopes to track sediments-derived inputs of the Kerguelen Plateau, Biogeosciences, Biogeosciences Discuss., 11, 14023-14061, 2014 Sandwell, D.T, and Zhang, B. Global mesoscale variability from

the Geosat exact repeat mission: Correlation with ocean depth, Journal of Geophysical Research, 94, 17, 971–17,984, doi:10.1029/JC094iC12p17971, 1989.

Sansone F.J. and Martens, C.S. Methane oxidation in Cape Lookout Bight, North Carolina, Limnology and Oceanography, 23, 349–355, 1978.

Sansone, F.J., Popp, B.N. ,Gasc, A. Graham, W. Rust, T.M. Highly elevated methane in the eastern tropical North Pacific and associated isotopically enriched fluxes to the atmosphere, Geophysical Research Letters, 28 4567–4570, 2001.

Sarmiento, J.L. and Gruber, N. Ocean Biogeochemical Dynamics. Princeton University Press, 2006.

Scranton, M.I and Brewer, P. Occurrence of methane in the near-surface waters of the western subtropical North Atlantic, Deep-Sea Research, 24, 127-138, 1977.

Simó, R., Archer, S.D., Pedró-Alió, C., Gilpin, L., Stelfox-Widdicombe, C.E. Coupled dynamics of dimethyl- sulfoniopropionate and dimethylsulfide cycling and the microbial food web in surface waters of the North Atlantic, Limnology and Oceanography, 47, 53–61, 2002.

Sun, J., Steindler, L. J. Thrash, C. , Halsey, K.H., Smith, D.P. Amy E. Carter, A.E. , Zachary C. Landry,Stephen J. Giovannoni. One Carbon Metabolism in SAR11 Pelagic Marine Bacteria. PloS one DOI: 10.1371/journal.pone.0023973, 2011.

Tilbrook, E.D and Karl, D.M. Dissolved methane distributions, sources, and sinks in the western Bransfield Strait, Antarctica, Journal of Geophysical Research, 99, 16383–16393, 1994.

Tréguer P, Le Corre P Manuel d'analyse des sels nutritifs dans I'eau de mer Uti:lisation de 1'AutoAnalyzt-r 2 Technicon, 2nd edn. 'Univ Bretagne occidentale, Brest, 1975.

Turner, S.M., Harvey, M. J., Law, C. S., Nightingale, P.D and Liss P.S. Iron-induced changes in oceanic sulfur biogeochemistry, Geophysical Research Letter, 31, L14307, doi:10.1029/2004GL020296, 2004.

van der Merwe, P., Bowie, A.R., Quéroué, F., Armand, L., Blain, S., Chever, F., Davies, D., Dehairs, F., Planchon, F., Sarthou, G. et al., 2014. Sourcing the iron in the naturally-fertilised bloom around the Kerguelen Plateau: particulate trace metal dynamics Biogeosciences Discussion, 11: 13389–13432, doi:10.5194/bgd-11-13389, 2014.

Vila-Costa, M., Simó, R., Harada, H., Gasol, J.M., Slezak D. and Kiene, R.P. Dimethylsulfoniopropinate uptake by marine phytoplankton, Science, 314, 652, 2006.

Vissher, P.T. ,Kiene, R.P., Taylor B.F. Demethylation and cleavage of demethylsulfoniopropionate in marine intertidal sediments, FEMS Microbiology Ecology, 14 179–190, 1994.

Walter, S., Peeken, I., Lochte, K and Bange, H.W. Nitrous oxide measurements during EIFEX, the European Iron Fertilisation Experiment in the subpolar South Atlantic Ocean, Geophysical Research Letter, 32, L23613,doi: 10.1029/2005GL024619, 2005.

Wingenter, O.W., Haase, K.B., Strutton, P., Friedrich, G., Meinardi, S., Blake, D.R and Rowland, F. S. Changing concentrations of CO, $CH_4$, $C_5H8$, $CH_3Bt$, $CH_3I$ and dimethyl sulfide during the Southern Ocean Iron Enrichment Experiments, Proceedings of the National Academy of Sciences101, 8537–8541, 2004.

Wanninkhof, R. Relationship between wind speed and gas exchange over the ocean, Journal Geophysical Research, 97, 7373-7382, 1992.

Weisenburg, D.A and Guinasso, N.L. Equilibrium solubilities of methane, carbon monoxide and hydrogen in water and seawater, Journal of Chemical Engineering Data, 24, 354-360, 1979.

Weiss, R.F. and Prince, B. A. Nitrous oxide solubility in water and seawater, Marine Chemistry 8, 347-359, 1980.

Weller D.I ., Law, C.S., A. Marriner, A., Nodder S.D., Chang, F.H., Stephens, J.A., Wilhelm S.W., Boyd P.W., Sutton P.J.H. Temporal variation of dissolved methane in a subtropical mesoscale eddy during a phytoplankton bloom in the southwest Pacific Ocean, Progress in Oceanography., 116, 193–206, 2013.

Wolfe, R.S. Microbial formation of methane, Advance Microbial Physiology, 6, 107–146, 1971.

Wuebbles, D.J and Hayhoe, K. Atmospheric methane and global change, Earth-Science Reviews, 57, 177–210, 2002.

Yoch, D. Dimethylsulfoniopropionate: Its Sources, Role in the Marine Food Web, and Biological Degradation to Dimethylsulfide Applied Environmental Microbiology 2002; 68(12), 5804–5815, 2002. doi: 10.1128/AEM.68.12.5804-5815, 2002.

Yoshida, O., Inoue,H. Y., Watanabe, S, Suzuki, K. and Noriki, S. Dissolved methane distribution in the South Pacific and the Southern Ocean in austral summer J. Geophysical Research 116, C07008, 2011, doi:10.1029/2009JC006089, 2011.

Zhang, Y., Lacan, F. and Jeandel, C. Dissolved rare earth elements tracing lithogenic inputs over the Kerguelen Plateau (Southern Ocean), Deep Sea Research Part II: Topical Studies in Oceanography, 55(5-7), 638, 2008.

Zhou, M., Zhu, Y., d'Ovidio, F., Park, Y.-H., Durand, I., Kestenare, E., Sanial, V., Van-Beek, P., Queguiner, B., Carlotti, F., and Blain, S.: Surface currents and upwelling in Kerguelen Plateau regions, Biogeosciences Discussion, 11, 6845–6876, 2014.

**Figure caption**

Figure 1. Map showing the location of biogeochemical stations sampled during the KEOPS 2 cruise. Bathymetric topography is shown in the main oceanographic region. The orange line delimits the position of the polar front. The sampled transects are indicated.

Figure 2. Left column: a)Temperature (T°C), c)Salinity and e) T-S diagram for W-E transect. Station located under the influence of PFZ (purple) is shown, showing enhanced water mass mixing. Arrows indicate position of PF crossing this transect. Right column: b)Temperature(T°C), d) Salinity and f) T-S diagram for W-E transect.

Figure 3. Vertical cross section of a) nitrate (µmol $L^{-1}$); b) phosphate (µmol $L^{-1}$); c) chlorophyll-a (µg $L^{-1}$); d) dissolved oxygen (µmol $L^{-1}$), e) nitrous oxide (nmol $L^{-1}$) and f) methane (nmol $L^{-1}$) for for zonal transect between 69-75°E. Arrows indicate position of PF crossing this transect

Figure 4. Vertical cross section of a) nitrate (µmol $L^{-1}$); b) phosphate (µmol $L^{-1}$); c) chlorophyll-a (µg $L^{-1}$); d) dissolved oxygen (µmol $L^{-1}$), e) nitrous oxide (nmol $L^{-1}$); f) methane (nmol $L^{-1}$) for the meridional transect between 45°-51°S.

Figure 5. PCA analysis with environmental data including dissolved iron obtained in the zonal transect (TWE). PCA comprises a) data from the surface to the ML´s base and b) environmental data from the surface to 500 m depth. Stations along with the eigenvectors are included.

Figure 6. Vertical distribution of biogeochemical variables from selected stations. Different biogeochemical regimes are defined as HNLC area (St. R), northern and southern area of Polar front (St. NS01 and A3) and within the Polar front (Sts. TWE03 and TWE07).

Table 1. General oceanographic features of the sampled stations during the KEOPS 2 cruise

| Biogeochemical Provinces | Stations | Latitude °E | Longitude °S | Date mm-dd-yy | Bottom Depth (m) | MLD (m) | Temperature (ºC) | Salinity | Oxygen (µmol/Kg) |
|---|---|---|---|---|---|---|---|---|---|
| | **OISO-6** | -44.59 | 52.06 | 10-15-11 | 3260 | 110 | 3.68 (3.66-3.68) | 33.80 (33.80-33.81) | 317.4 (314-318) |
| | **OISO-7** | -47-4 | 58.00 | 10-16-11 | 4300 | 127 | 4.75 (4.73-4.76) | 33.79 (33.8-33.81) | 308.4 (305-309) |
| **N-S transect** | | | | | | | | | |
| | **A3-1** | -50,38 | 72.05 | 10-19-11 | 535 | 181 | 1.68 (1.68-1.73) | 33.89 (33.85-33.91) | 325.9 (321-327) |
| | **A3-2** | -50.38 | 72.05 | 10-16-11 | 527 | 165 | 2.16 (2.10-2.18) | 33.91 (33.911-33.913) | 333.2 (329-335) |
| | **TNS10** | -50.12 | 72.07 | 10-21-11 | 565 | 163 | 1.67 (1.59-1.68) | 33.90 (33.80-33.93) | 325.9 (314-327) |
| Eddy | **TNS09** | -49.47 | 72.12 | 10-21-11 | 615 | 137 | 1.75(1.66-1.89) | 33.91(33.80-33.84) | 321.1 (265-331) |
| Eddy | **TNS08** | -49.27 | 72.14 | 10-21-11 | 1030 | 139 | 2.11 (2.06-2.12) | 33.869 (33.86-33.87) | 329.4 (324-328) |
| | **TNS07** | -49.08 | 72.17 | 10-22-11 | 1890 | 62 | 2.10 (1.95-2.16) | 33.86 (33.86-33.87) | 327.7 (327-331) |
| | **TNS06** | -48.48 | 71.18 | 10-22-11 | 1885 | 67 | 2.32 (2.23-2.42) | 33.846 (33.84-33.85) | 327.6 (315-316) |
| | **TNSO5** | -48.28 | 72.12 | 10-22-11 | 2060 | 114 | 2.22 (2.09-2.26) | 33.85 (33.85-33.86) | 326.7(323-328) |
| | **TNS03** | -47.05 | 71.55 | 10-23-11 | 540 | 111 | 2.17 (2.06-2.26) | 33.89(33.88-33.89) | 307.6(304-310) |
| | **TNS02** | -47.19 | 71.42 | 10-23-11 | 520 | 65 | 3.60 (3.38-3.67) | 33.69 (33.68-33.69) | 318.6 (317-319) |
| | **TNS01** | -46,.49 | 71.30 | 10-23-11 | 2280 | 45 | 4.02(3.96 -4.13) | 33.71(33.71-33.72) | 316.1 (315-318) |
| **HNLC** | **RK2-2** | -50.21 | 66.43 | 10-23-11 | 2300 | 111 | 2.11 (2.06-2.14) | 33.78 (33.77-33.78) | 326.7 (326-327) |
| **E-W transect** | | | | | | | | | |
| **(Shelf)** | **TEW1** | -49,08 | 69.50 | 10-31-11 | 86 | 16 | 3.27 (3.17-3.36) | 33.61(33.61-33.62) | 344.16 (340-345) |
| **(Shelf)** | **TEW2** | -48,53 | 70.39 | 10-31-11 | 84 | 40 | 2.55 (2.49-2.68) | 33.75 (33.75-33.76) | 332,0 (327-337) |
| **(Shelf)** | **TEW3** | -48,47 | 71.01 | 10-31-11 | 565 | 62 | 2.17 (2.12-2.31) | 33.86 (33.86-33.87) | 329.69 (328-331) |
| **(NPF)** | **TEW4** | -48,37 | 71.28 | 11-01-11 | 1585 | 95 | 2.54 (2.41-2.60) | 33.85 (33.85-33.86) | 334.60 (331-337) |
| | **TEW5** | -48,28 | 72.47 | 11-01-11 | 2275 | 60 | 2.51 (2.39-2.60) | 33.84 (33.84-33.85) | 331.42 (327-336) |
| **(SPF)** | **TEW7** | -48,27 | 73.59 | 11-02-11 | 2510 | 17 | 4.02 (3.91-4.10) | 33.78 (33.784-33.79) | 315.95 (346-349) |
| | **TEW8** | -48,28 | 75.19 | 11-02-11 | 2786 | 22 | 4.15 (4.08-4.18) | 33.76 (33.76-33.77) | 338.75(347-350) |
| **Time Series Stations** | | | | | | | | | |
| | **E1-1** | -48.27 | 72.11 | 10-28-11 | 2056 | 84 | 2.48 (2.36-2.54) | 33.85(33.84-33.85) | 331.54(328-333) |
| | **E1-2** | -48.31 | 72.04 | 11-01-11 | 2003 | 42 | 2.42 (2.28-2.56) | 33.85 (33.85-33.86) | 331.68 (329-333) |
| | **E1-3** | -48.41 | 71.58 | 11-03-11 | 1915 | 41 | 2.74 (2.60-2.81) | 33.84 (33.84-33.85) | 332.08 (331-332) |
| | **E1-4W** | -48.45 | 71.25 | 11-11-11 | 1384 | 67 | 2.36 (2.07-2.51) | 33.90 (33.90-33.91) | 329.95 (326-332) |
| | **E1-4E** | -48.42 | 72.33 | 11-12-11 | 2210 | 77 | 3.15 (2.78-3.19) | 33.84 (33.83-33.85) | 329.89 (326-331) |
| | **E1-5** | -48.24 | 71.50 | 11-18-11 | 1920 | 36 | 2.53 (2.50-2.62) | 33.85 (33.85-33.85) | 326.97(330-333) |

Table 2. Inventories of gases and nutrients estimated in the mixed layer (ML) and the entire water column, along with GHG concentrations, wind velocities and concomitant estimated gas exchange across the air-sea interface

| Station | Inventory in the MLD | | | | | Inventory in the Water Column | | | | GHGs | | Wind | Flux LM86 | | Flux W92 | |
|---|---|---|---|---|---|---|---|---|---|---|---|---|---|---|---|---|
| | *Chl-a | $CH_4$ | $N_2O$ | $NO_3^-$ | $PO_4^{3-}$ | $N_2O$ | $CH_4$ | $NO_3$- | $PO_4^{3-}$ | $N_2O$ | $CH_4$ | | $N_2O$ | $CH_4$ | $N_2O$ | $CH_4$ |
| | mg $m^{-2}$ | mmol $m^{-2}$ | mmol $m^{-2}$ | mol $m^{-2}$ | mol $m^{-2}$ | mmol $m^{-2}$ | mmol $m^{-2}$ | mol $m^{-2}$ | mol $m^{-2}$ | nM | nM | m $s^{-1}$ | µmol $m^{-2}$ $d^{-1}$ | | µmol $m^{-2}$ $d^{-1}$ | |
| **N-S Transect** | | | | | | | | | | | | | | | | |
| **A3-1** | 12.60 | 3.00 | 2.43 | 5.41 | 0.293 | 5.72 | 4.12 | 7.342 | 0.940 | 13.73 | 6.56 | 6.58 | -1.54 | 18,75 | -2.96 | 35.93 |
| **A3-2** | 35.48 | 3.31 | 1.81 | 4.38 | 0.300 | 5.273 | 3.31 | 15.04 | 1.024 | 11.64 | 8,,37 | 11.39 | -10.5 | 14.24 | -22.9 | 29.70 |
| **TNS10** | 14.09 | 1.39 | 2.56 | 4.79 | 0.319 | 9.29 | 2.17 | 16.03 | 1.077 | 15.49 | 7.79 | 12.66 | 3.57 | 14.90 | 6.56 | 27.48 |
| **TNS09** | 35.58 | 1.33 | 2.23 | 3.91 | 0.254 | 7.51 | 1.87 | 12.53 | 0.864 | 15.89 | 14.54 | 14.38 | 5.08 | 38.10 | 9.36 | 70.26 |
| **TNS08** | 23.23 | 0.68 | 2.16 | 3.98 | 0.260 | 9.27 | 1.58 | 15.75 | 1.038 | 15.46 | 5.65 | 11.89 | 4.29 | 7.80 | 7.92 | 14.38 |
| **TNS07** | 25.45 | 0.25 | 1.02 | 1.69 | 0.111 | 9.99 | 1.80 | 15.74 | 1.072 | 16.92 | 4.01 | 11.89 | 8.65 | 2.03 | 15.55 | 3.66 |
| **TNS06** | 16.33 | 0.57 | 0.92 | 1.83 | 0.123 | 8.65 | 2.54 | 15.93 | 1.070 | 13.81 | 8.74 | 11.89 | -0.78 | 17.59 | -1.20 | 31.64 |
| **TNSO5** | 17.19 | 0.74 | 1.68 | 3.07 | 0.212 | 9.27 | 2.46 | 15.39 | 1.070 | 14.67 | 6.41 | 11.40 | 1.81 | 9.91 | 3.26 | 17.82 |
| **TNS03** | 17.28 | 0.88 | 1.75 | 3.06 | 0.214 | 7.75 | 3.14 | 12.46 | 0.875 | 11.05 | 7.23 | 11.40 | 4.13 | 9.93 | 6.85 | 16.44 |
| **TNS02** | 11.25 | 0.26 | 0.91 | 1.73 | 0.123 | 8.27 | 1.57 | 15.08 | 1.046 | 13.92 | 4.38 | 9.73 | 1.48 | 3.03 | 2.45 | 5.00 |
| **TNS1** | 11.21 | 0.39 | 0.63 | 1.07 | 0.076 | 8.89 | 3.16 | 14.17 | 0.976 | 13.95 | 8.48 | 9.73 | 2.26 | 14.40 | 3.74 | 23.84 |
| **RK2-2** | 14.89 | 0.64 | 1.63 | 2.79 | 0.197 | 2.83 | 1.06 | 4.900 | 0.347 | 14.83 | 6.29 | 6.86 | 0.89 | 4.09 | 1.34 | 6.15 |
| **W-E Transect** | | | | | | | | | | | | | | | | |
| **TEW1** | 9.78 | 0.19 | 0.26 | 3.40 | 0.412 | 1.18 | 1.30 | 1.560 | 0.111 | 15.29 | 9.50 | 4.60 | 0.87 | 3.15 | 1.69 | 6.15 |
| **TEW2** | 9.87 | 0.43 | 0.62 | 0.84 | 1.073 | 1.12 | 1.74 | 1.873 | 0.133 | 15.03 | 9.88 | 4.60 | 0.54 | 3.24 | 1.06 | 6.33 |
| **TEW3** | 8.77 | 0.73 | 0.91 | 0.51 | 1.566 | 7.41 | 2.40 | 14.97 | 1.072 | 15.56 | 14.09 | 4.60 | 0.67 | 5.25 | 1.32 | 10.24 |
| **E1-2** | 15.33 | 0.52 | 0.20 | 0.82 | 1.167 | 9.78 | 2.80 | 15.24 | 1.051 | 14.95 | 11.42 | 6.92 | 1.34 | 11.67 | 2.01 | 17.57 |
| **TEW4** | 35.53 | 0.40 | 1.63 | 0.30 | 2.468 | 10.3 | 1.81 | 15.74 | 1.106 | 16.62 | 3.50 | 6.92 | 3.76 | 0.21 | 5.67 | 0.32 |
| **TEW5** | 23.11 | 0.38 | 0.99 | 0.52 | 1.619 | 10.21 | 2.61 | 15.62 | 1.099 | 16.31 | 6.35 | 6.92 | 3.28 | 4.34 | 4.94 | 6.54 |
| **TEW7** | 75.45 | 0.19 | 0.23 | 2.39 | 0.353 | 9.26 | 7.44 | 15.23 | 1.087 | 12.90 | 10.87 | 8.04 | -0.96 | 15.42 | -1.52 | 23.78 |
| TEW8 | 59.52 | 0.10 | 0.37 | 1.52 | 0.472 | 10.05 | 1.59 | 15.27 | 1.058 | 15.77 | 4.95 | 8.04 | 5.25 | 3.52 | 8.10 | 5.42 |

*Inventories estimated from the photic zone

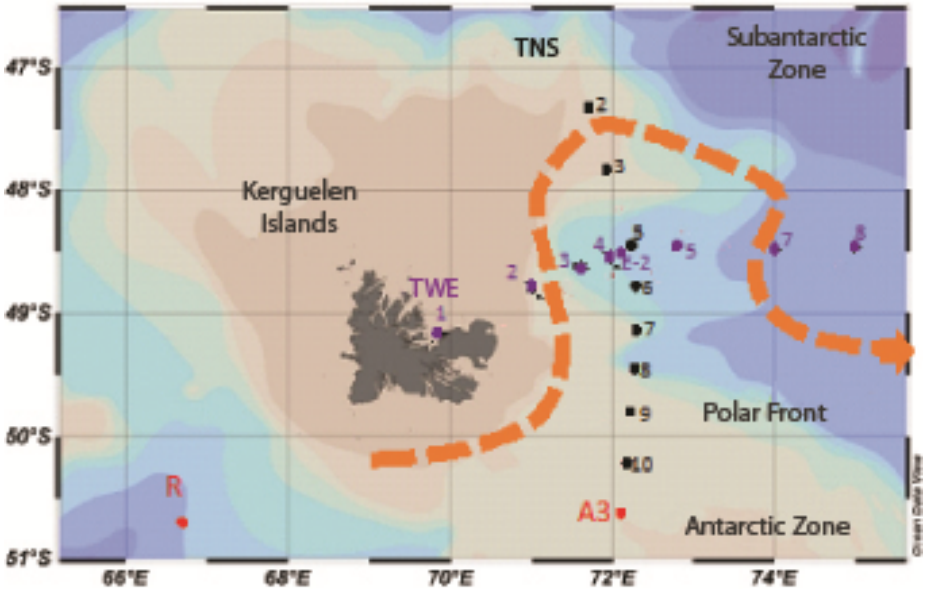
TNS
Subantarctic Zone
Kerguelen Islands
TWE
Polar Front
Antarctic Zone
R
A3
47°S
48°S
49°S
50°S
51°S
66°E
68°E
70°E
72°E
74°E

Figure 1

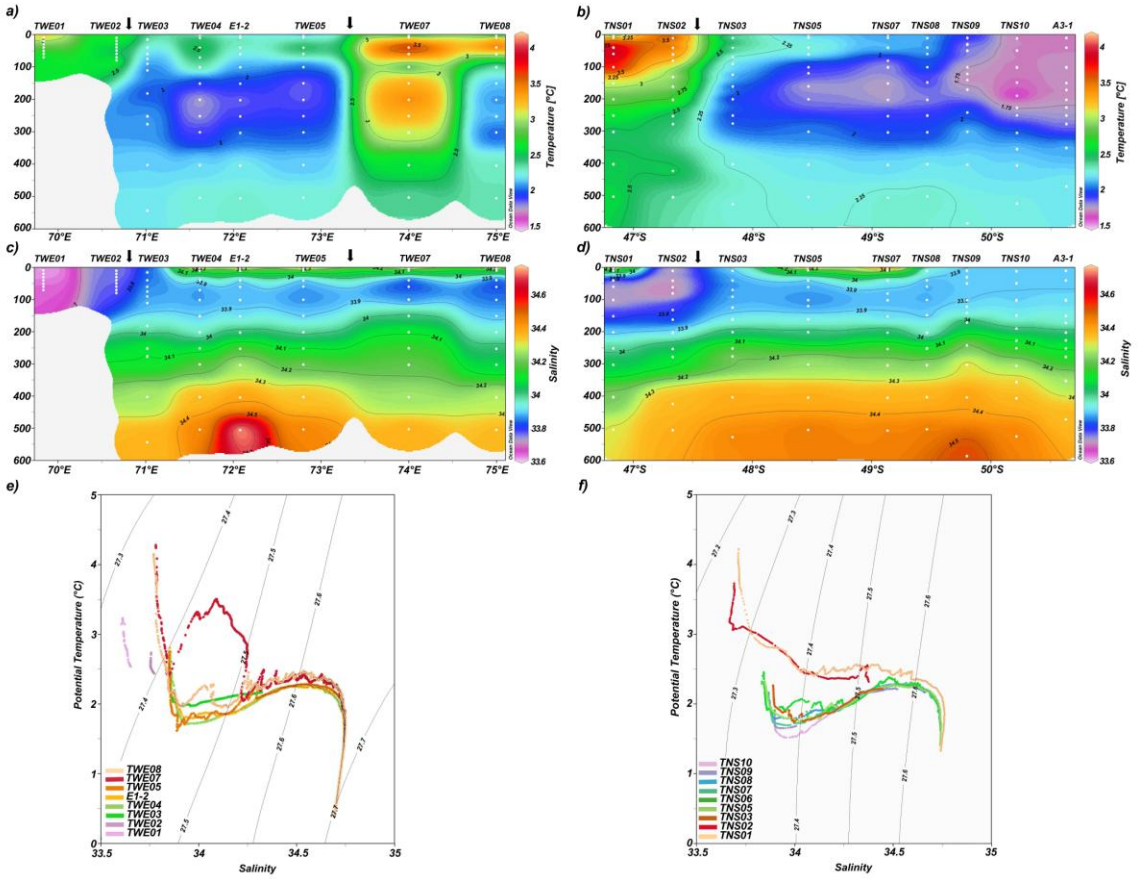
a)
TWE01 TWE02 TWE03 TWE04 E1-2 TWE05 TWE07 TWE08
70°E 71°E 72°E 73°E 74°E 75°E
Temperature [°C]
b)
TNS01 TNS02 TNS03 TNS05 TNS07 TNS08 TNS09 TNS10 A3-1
47°S 48°S 49°S 50°S
Temperature [°C]
c)
TWE01 TWE02 TWE03 TWE04 E1-2 TWE05 TWE07 TWE08
70°E 71°E 72°E 73°E 74°E 75°E
Salinity
d)
TNS01 TNS02 TNS03 TNS05 TNS07 TNS08 TNS09 TNS10 A3-1
47°S 48°S 49°S 50°S
Salinity
e)
Potential Temperature (°C)
Salinity
TWE08
TWE07
TWE05
E1-2
TWE04
TWE03
TWE02
TWE01
f)
Potential Temperature (°C)
Salinity
TNS10
TNS09
TNS08
TNS07
TNS06
TNS05
TNS03
TNS02
TNS01

Fig 2

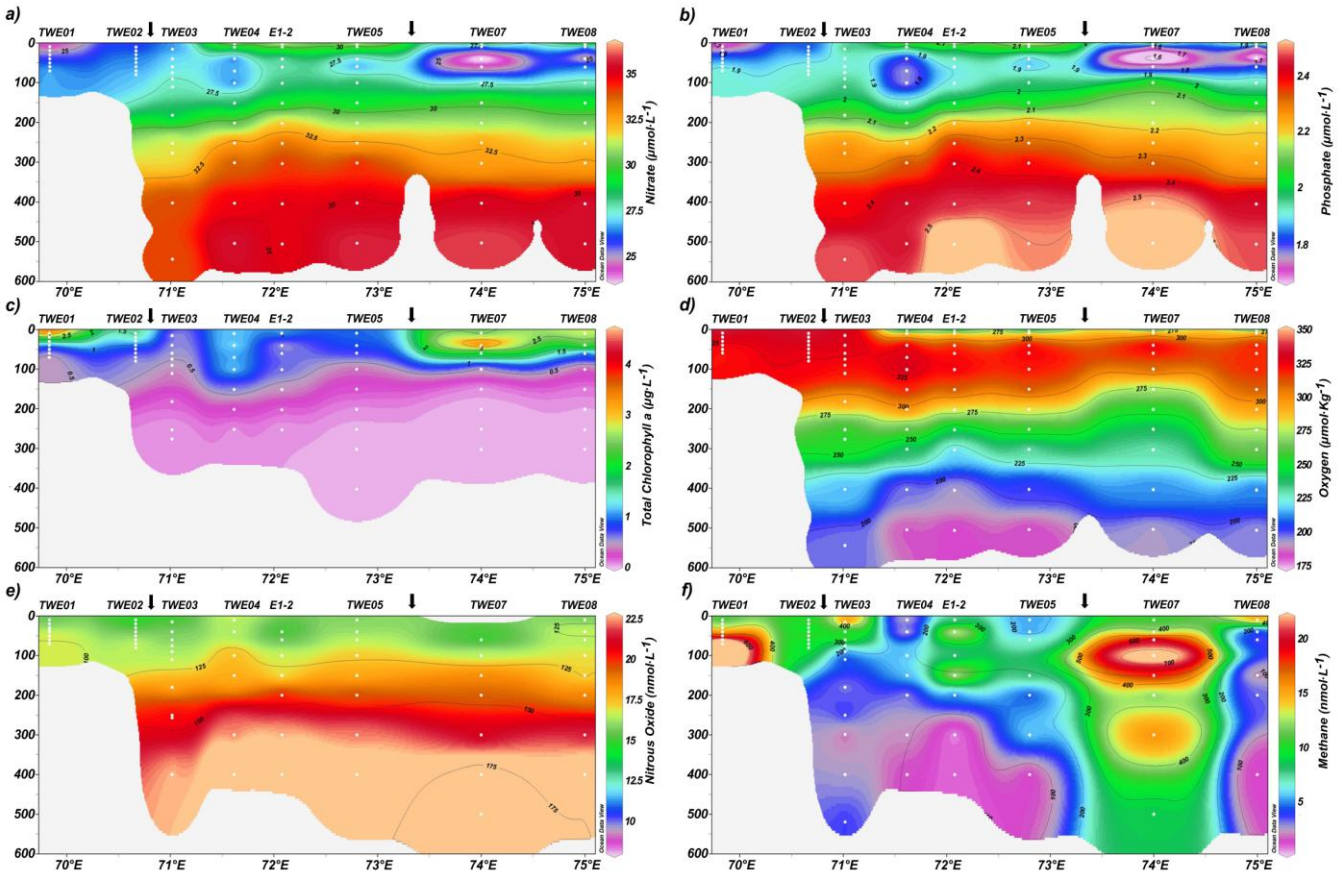
a)
b)
c)
d)
e)
f)
TWE01
TWE02
TWE03
TWE04
E1-2
TWE05
TWE07
TWE08
70°E
71°E
72°E
73°E
74°E
75°E
Nitrate (µmol·L⁻¹)
Phosphate (µmol·L⁻¹)
Total Chlorophyll a (µg·L⁻¹)
Oxygen (µmol·Kg⁻¹)
Nitrous Oxide (nmol·L⁻¹)
Methane (nmol·L⁻¹)

Fig 3

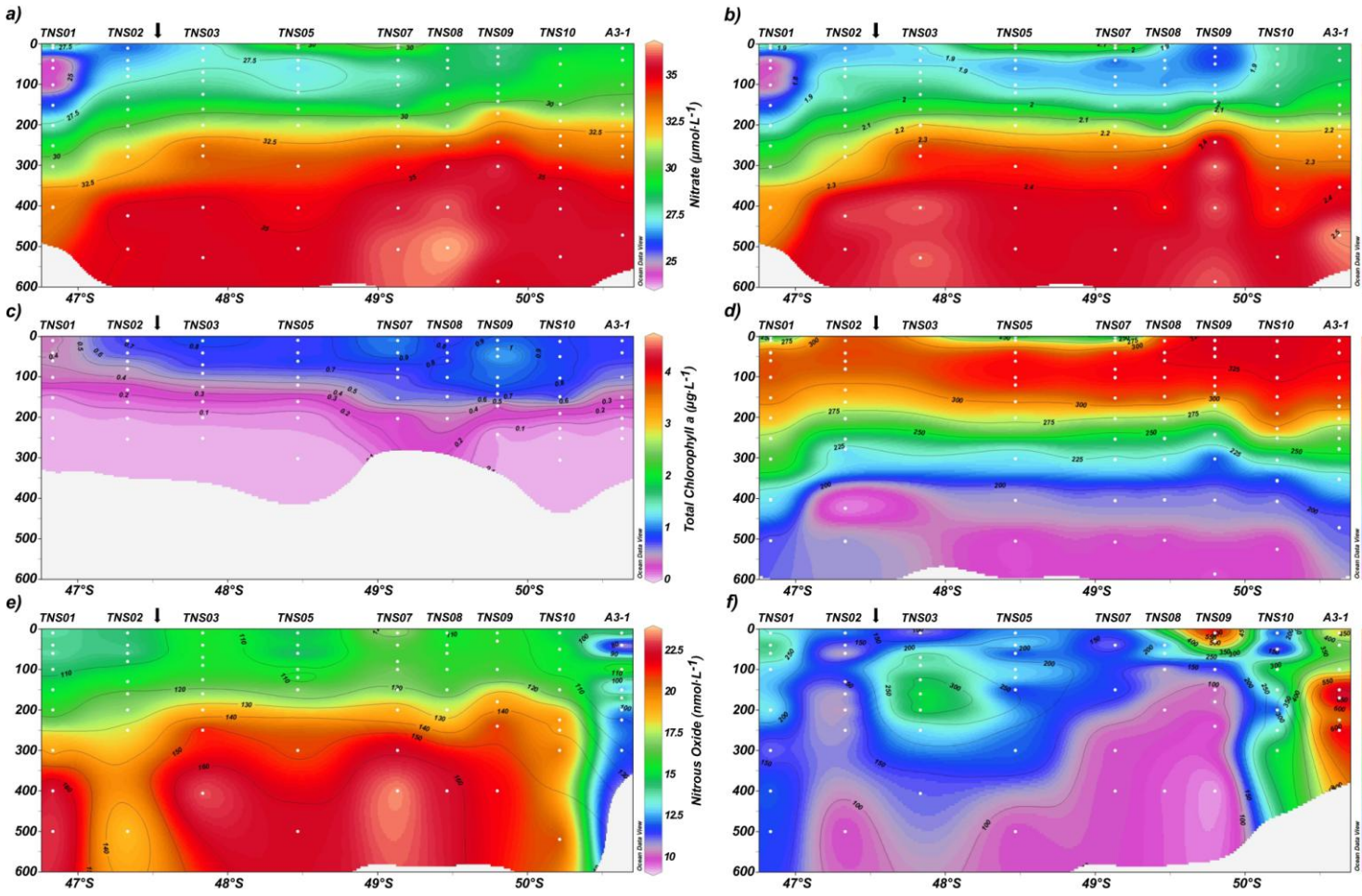
a)
b)
c)
d)
e)
f)
TNS01
TNS02
TNS03
TNS05
TNS07
TNS08
TNS09
TNS10
A3-1
47°S
48°S
49°S
50°S
Nitrate (µmol·L-1)
Total Chlorophyll a (µg·L-1)
Nitrous Oxide (nmol·L-1)

Fig 4

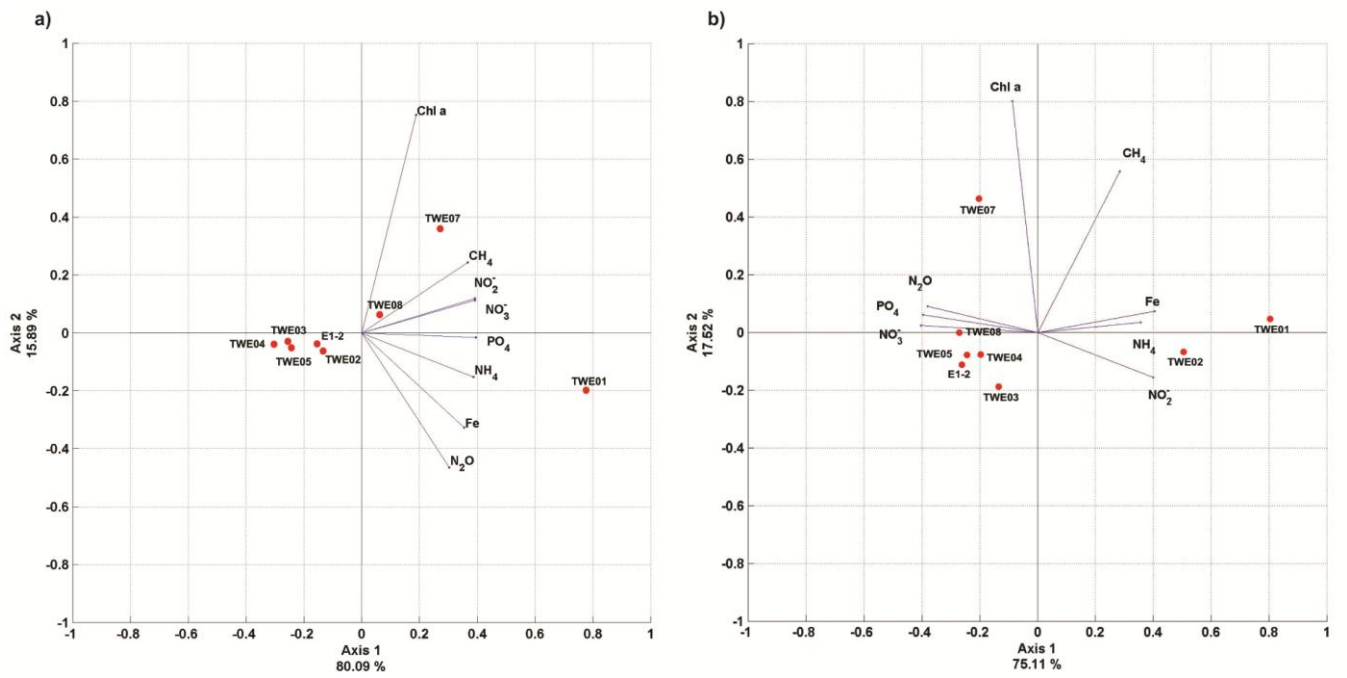
a)
Chl a
TWE07
CH4
NO2-
NO3-
TWE08
PO4
NH4
TWE01
Fe
N2O
TWE03
E1-2
TWE04
TWE05
TWE02
Axis 2
15.89 %
Axis 1
80.09 %
b)
Chl a
CH4
TWE07
N2O
PO4
Fe
NO3-
TWE08
TWE01
NH4
TWE02
TWE05
TWE04
E1-2
TWE03
NO2-
Axis 2
17.52 %
Axis 1
75.11 %

Fig. 5

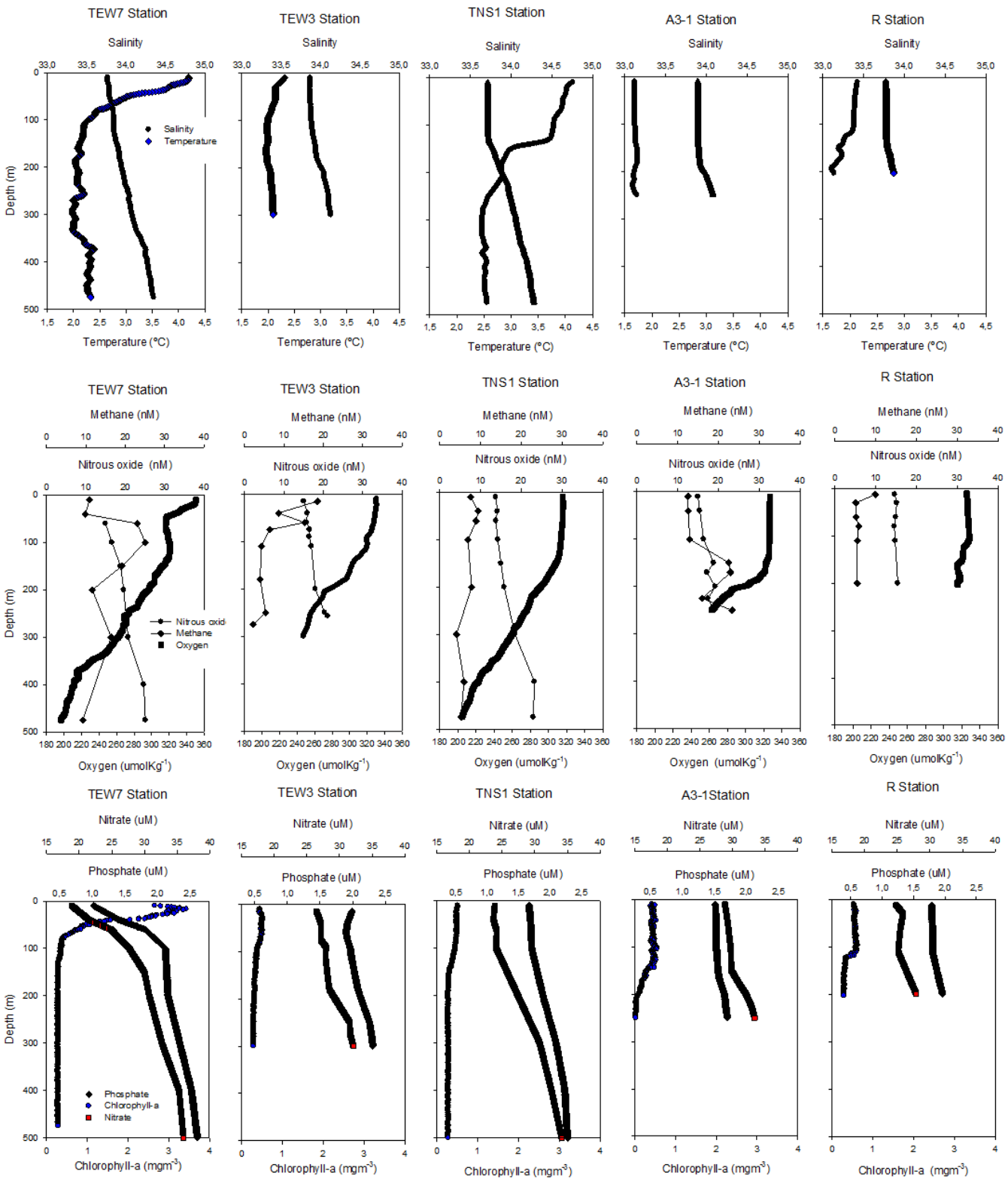
TEW7 Station
TEW3 Station
TNS1 Station
A3-1 Station
R Station
Salinity
Temperature (°C)
Depth (m)
Methane (nM)
Nitrous oxide (nM)
Oxygen (umolKg-1)
Nitrate (uM)
Phosphate (uM)
Chlorophyll-a (mgm-3)
A3-1Station

Fig. 6